Kinetics, SOA yields and chemical composition of secondary organic aerosol from β-caryophyllene ozonolysis with and without nitrogen oxides between 213 and 313 K

Linyu Gao[1,2], Junwei Song[1,2], Claudia Mohr[3], Wei Huang[4], Magdalena Vallon[1], Feng Jiang[1,2], Thomas Leisner[1,5], and Harald Saathoff[1]

[1] Institute of Meteorology and Climate Research, Karlsruhe Institute of Technology, Karlsruhe, Germany
[2] Institute of Geography and Geoecology, Working Group for Environmental Mineralogy and Environmental System Analysis, Karlsruhe Institute of Technology, Karlsruhe, Germany
[3] Department of Environmental Science, Stockholm University, Stockholm, Sweden
[4] Institute for Atmospheric and Earth System Research / Physics, Faculty of Science, University of Helsinki, Helsinki, Finland
5. Institute of Environmental Physics, Heidelberg University, Heidelberg, Germany

Correspondence to: Linyu Gao (linyu.gao@kit.edu) and Dr. Harald Saathoff (harald.saathoff@kit.edu)

Abstract.β-caryophyllene (BCP) is one of the most important sesquiterpenes (SQTs) in the atmosphere, with a large potential contribution to secondary organic aerosol (SOA) formation mainly from reactions with ozone (O_3) and nitrate radicals (NO_3). In this work, we study the temperature dependence of the kinetics of BCP ozonolysis, SOA yields, and SOA chemical composition in the dark and in the absence and presence of nitrogen oxides including nitrate radicals (NO_3). We cover a temperature range of 213K – 313K, representative of tropospheric conditions. The oxidized components in both gas and particle phases were characterized on a molecular level by a Chemical Ionization Mass Spectrometer equipped with a Filter Inlet for Gases and AEROsols using iodide as the reagent ion (FIGAERO-iodide-CIMS). The batch mode experiments were conducted in the 84.5 m^3 aluminium simulation chamber AIDA at the Karlsruhe Institute of Technology (KIT). In the absence of nitrogen oxides, the temperature-dependent rate coefficient of the endocyclic double bond in BCP reacting with ozone between 243 – 313 K are negatively correlated with temperature, corresponding to the following Arrhenius equation: $k = (1.6\pm0.4) \times10^{-15} \times exp((559\pm97)/T)$. The SOA yields increase from 16±5 % to 37±11% with temperatures decreasing from 313 K to 243 K at a total organic particle mass of 10 µg m^{-3}. The variation of the ozonolysis temperature leads to a substantial impact on the abundance of individual organic molecules. In the absence of nitrogen oxides, monomers $C_{14-15}H_{22-24}O_{3-7}$ (37.4 %), dimers $C_{28-30}H_{44-48}O_{5-9}$ (53.7 %) and trimers $C_{41-44}H_{62-66}O_{9-11}$ (8.6 %) are abundant in the particle phase at 213K. At 313K, we observed more oxidized monomers (mainly $C_{14-15}H_{22-24}O_{6-9}$, 67.5 %) and dimers (mainly $C_{27-29}H_{42-44}O_{9-11}$, 27.6 %), including highly oxidized molecules (HOMs, $C_{14}H_{22}O_{7,9}$, $C_{15}H_{22}O_{7,9}$ $C_{15}H_{24}O_{7,9}$) which can be formed via hydrogen shift mechanisms, but no significant trimers. In presence of nitrogen oxides, the organonitrate fraction increased from 3 % at 213K to 12 % and 49 % at 243K and 313K, respectively. Most of the organonitrates were monomers with C_{15} skeletons and only one nitrate group. Higher oxygenated organonitrates were observed at higher temperatures, with their signal-weighted O:C atomic ratio increasing from 0.41 to 0.51 from 213K to 313K. New dimeric and trimeric organic species without nitrogen atoms (C_{20}, C_{35}) were formed in presence of nitrogen oxides at 298-313K indicating potential new reaction pathways. Overall, our results show that increasing temperatures lead to a relatively small decrease of the rate coefficient of the endocyclic double bond in BCP reacting with ozone, but to a strong decrease in SOA yields. In contrast, the formation of HOMs and organonitrates increases significantly with temperature.

1 Introduction

Biogenic volatile organic compounds (BVOCs), which are emitted mainly from plants, are the largest source of precursors of atmospheric secondary organic aerosol (SOA), which has profound impacts on visibility, air quality, human health, clouds and climate change (Fehsenfeld et al., 1992; Mellouki et al., 2015; Laothawornkitkul et al., 2009; Charnawskas et al., 2017).

45 Sesquiterpenes (SQTs, $C_{15}H_{24}$), are a class of BVOCs mainly emitted from coniferous trees (Kleist et al., 2012; Matsunaga et al., 2013), scots pines (Kivimäenpää et al., 2020; Weikl et al., 2016), and deciduous trees (Li et al., 2019). Despite their lower atmospheric emission concentrations compared to isoprene and monoterpenes (Faiola et al., 2018), SQTs are important in the atmosphere because of their high reactivities with ozone and large aerosol formation potentials (Ciccioli et al., 1999; Lee et al., 2006a; Lee et al., 2006b; Ng et al., 2007). Depending on 50 region and season they can even play a dominating role (Geron and Arnts, 2010; Tarvainen et al., 2005; Jardine et al., 2011; Shrivastava et al., 2019).

Among all the sesquiterpene species, β-caryophyllene (BCP) is one of the most abundant and is emitted e.g. from various pine trees, but also from plants used for agricultural purposes (Duhl et al., 2008), like foliage of orange trees (Ciccioli et al., 1999; Hansen and Seufert, 2003), potato plants (Agelopoulos et al., 2000), and cotton 55 (Rodriguez-Saona et al., 2001). BCP is a bicyclic compound with two double bonds with different reactivities towards ozone. The rate coefficient for ozone reacting with the endocyclic double bond at 296 K was determined as $(1.2 \pm 0.4) \times 10^{-14}$ cm^3 molecule^{-1} s^{-1} (Shu and Atkinson, 1994; Richters et al., 2015). It is estimated to be about 100 times larger than the rate coefficient of $(1.1 \pm 0.4) \times 10^{-16}$ cm^3 molecule^{-1} s^{-1} for the exocyclic double bond (Shu and Atkinson, 1994) of the first-generation products. Therefore, the atmospheric lifetime of the endocyclic 60 double bond towards ozone is estimated to about 2 minutes, and the first-generation products can exist about 3.5 hours in typical tropospheric ozone levels of 30 ppb (Winterhalter et al., 2009).

The SOA mass yield of BCP ozonolysis is expected to be dependent on organic particle mass concentration (Odum et al., 1996), temperature (Saathoff et al., 2009) and ozone levels (Chen et al., 2012). Previous studies give a relatively large range of SOA yields of 5-70% depending on the experimental conditions (Jaoui et al. (2003), Lee 65 et al. (2006a), Winterhalter et al. (2009), Chen et al. (2012), Tasoglou and Pandis, 2015), for a temperature range of 287 – 298 K. A comparison of these studies is given in the supplementary information (cf. Table S1).

Yields, products, and mechanisms of BCP ozonolysis were investigated extensively for room temperature (Jaoui et al., 2003; Griffin et al., 1999; Lee et al., 2006a; Lee et al., 2006b; Winterhalter et al., 2009; Nguyen et al., 2009; Jenkin et al., 2012; Richters et al., 2016). The oxidation products mainly include aldehydes, small acids, acetone 70 in the gas phase (Grosjean et al., 1993; Calogirou et al., 1999; Zhao et al., 2010; Larsen et al., 1998), and ketones, aldehydes, alcohols and carboxylic acids in the particle phase (Dekermenjian, 1999; Lee et al., 2006a; Jaoui et al., 2003; van Eijck et al., 2013; Jaoui et al., 2007; Li et al., 2011; Alfarra et al., 2012). Major oxidation products identified are e.g. β-caryophyllonic acid ($C_{15}H_{24}O_3$), β-caryophyllinic acid ($C_{14}H_{22}O_4$, BCA), β-hydroxycaryophyllonic acid ($C_{15}H_{24}O_4$) (Table S3). BCA has also been used as a tracer to estimate the emissions 75 of BCP in the real atmosphere (Jaoui et al., 2007; Hu et al., 2008; Parshintsev et al., 2008; Haque et al., 2016; Verma et al., 2021; Cheng et al., 2021). In addition, highly oxidized multifunctional organic molecules (HOMs) were observed from BCP ozonolysis. Richters et al. (2016) studied their formation mechanism at 295 K in a free-jet flow system using isotopic labelling. Major HOMs identified are $C_{14-15}H_{22}O_7$, $C_{14-15}H_{22}O_9$, and $C_{15}H_{22}O_{11,13}$ (Richters et al., 2016).

80   SQT oxidation products are expected to have low or extremely low vapor pressures owing to their long carbon skeletons with multiple functional groups. For example, the saturation vapor pressure of β-caryophyllinic acid was estimated as low as 3.3×10^{-13} Pa (Li et al., 2011), which leads to a high condensation and SOA formation potential. As a consequence, these species are expected to play an important role in new particle formation (NPF) (Kirkby et al., 2016; Kammer et al., 2020; Huang et al., 2021).

85   Especially during night-time, the reaction between nitrate (NO_3) radicals and unsaturated hydrocarbons is of substantial importance and results in SOA formation. BCP has a high reactivity towards NO_3 radicals, with a rate coefficient of $(1.93 \pm 0.35) \times 10^{-11}$ cm^3 molecule^{-1}s^{-1} (Shu and Atkinson, 1995; Winterhalter et al., 2009; Calvert et al., 2008). SOA formation from BCP ozonolysis in the presence of NO_3 radicals has only been subject of few studies so far. SOA yields from dark reactions between BCP and NO_3 were estimated to be 1.46 and 0.91 for SOA

90   mass concentrations of 113.4 and 60.3 μg m^{-3}, respectively (Jaoui et al., 2013). The formation mechanism of several organic nitrates including $C_{15}H_{23,25}O_4N$ and $C_{15}H_{25}O_{6,7}N$ is described in the Master Chemical Mechanism (MCM v3.2) by Jenkin et al. (2012).

The troposphere covers a wide temperature range which dependents on the altitude from the planetary boundary layer (PBL) to the upper troposphere, latitude, and seasonal variations. Typically, the tropospheric temperatures

95   range between 300 K to 200 K. In summer, some regions can even reach to 318 K. BVOCs and their oxidation products are proposed to undergo transport from the PBL to the upper troposphere e.g. via convective systems typical for tropical regions (Andreae et al., 2018). In this conceptual picture of a potential aerosol life cycle the temperature dependence of the different processes involved is quite important. Besides, multiple studies have shown that SOA yields typically increase with decreasing temperature, e.g. for α-pinene and limonene ozonolysis

100   (Saathoff et al., 2009), β-pinene ozonolysis (Von Hessberg et al., 2009), and isoprene ozonolysis (Clark et al., 2016). In addition, at lower temperatures also semi volatile components can have a big condensation potential (Stolzenburg et al., 2018; Ye et al., 2019). Considering the potentially important role of BCP oxidation products in NPF and their high condensation and SOA formation potential as abovementioned, the temperature dependence of SOA formation from ozonolysis of BCP is, however, mainly unclear to date.

105   The objectives of this work were to study the temperature dependence on the kinetics, yields, and chemical composition distribution of the aerosol produced by the reaction of BCP with O_3 in the temperature range between 213 – 313 K. Furthermore, we investigated the impact of the presence of nitrogen oxides including NO_3 radicals on the SOA chemical composition and volatility.

2 Methodology

110   **2.1 Experimental conditions**

A schematic of the AIDA (Aerosol Interaction and Dynamics in the Atmosphere) simulation chamber at the Karlsruhe Institute of Technology (KIT) and the main instrumentation used in this work are shown in Fig. 1. The chamber is an 84.5 m^3 aluminium vessel equipped with a LED solar radiation simulator and with precisely controlled temperature, humidity, and gas mixtures. It is operated as a continuously stirred reactor with mixing

115   times of 1-2 minutes achieved using a fan about 1 m above the bottom (Saathoff et al., 2009). Wall and gas temperature inside the chamber are controlled at ±0.3 K over a wide range of temperatures (313-183 K) (Wagner et al., 2006). The pressure inside the chamber can be varied from 0.01 to 1000 hPa and the relative humidity (RH)

can be modified between close to zero to up to 100% and even supersaturated conditions (Möhler et al., 2003). Water vapor is measured in situ by a tuneable diode laser (TDL) hygrometer with an accuracy of ±5% and a calibrated reference dew point mirror hygrometer (MBW373LX, MBW Calibration Ltd.) with an accuracy of ±1% (Fahey et al., 2014).

The results presented in this work are from dark BCP ozonolysis experiments with or without addition of NO_2 from a campaign in November and December 2019 covering five different temperatures between 213 - 313 K. The experimental conditions are listed in Table 1. Two additional experiments were undertaken in March 2020 to study the rate coefficients of BCP reacting with ozone at 243 K and 258 K. BCP (98%, Carl Roth GmbH) was added to the AIDA chamber with a flow of 0.01 m^3/min of synthetic air saturated with its vapour at 298K. Please note that the BCP concentrations for the experiments at 213 K could not be measured due to the low vapour pressure and strong wall losses at lower temperatures (more details are given in section 2.2). Ozone was in all experiments typically in excess and generated by a silent discharge generator (Semozon 030.2, Sorbios) in pure oxygen (99.9999%). The relative humidity ranged from 96% to 13% for experiments at 213 K and 313 K, respectively. This corresponds to water vapor concentrations of 1 Pa (3.4 ×10^{14} cm^{-3}) at 213 K and 952 Pa (2.2 ×10^{17} cm^{-3}) at 313 K, respectively, and reflects the variability of the water vapour concentrations throughout the troposphere. At the initial phase of each experiment, BCP was depleted completely by ozonolysis and SOA was formed. The corresponding conditions are marked as 1a-5a in Table 1. Subsequently, NO_2 (1000 ppm of 99.5% purity in nitrogen 99.999%, Basi Schöberl GmbH) was added to the reaction mixture still containing an excess of ozone. A second step of SOA formation was then initialized by adding more BCP. This series of experiments is marked as 1b-5b in Table 1. Hence, the BCP and ozone concentrations listed in Table 1 for experiments 1b-5b include also the amounts added in experiments 1a-5a. Ozone was at nearly the same concentrations as for the initial experiments without NO_2, except for the experiments at 273 K. To get a slower decay of BCP to better determine its rate coefficient at 273K, we added 73 ppb ozone into the chamber first, and then added more ozone to the same concentration level (~300 ppb) as used for the other temperatures for comparison. All experiments were performed in the dark and no hydroxyl radical scavenger was used. Hence, the OH radicals generated in the ozonolysis reaction with a yield of (10.4 ± 2.3) % (Winterhalter et al., 2009) or 6% (Shu and Atkinson, 1994) also contributed to SOA formation as will be detailed in section 3.1. Time zero in the plots refers to the first addition of ozone to the reaction mixture.

2.2 Instrumentation

The main instruments used for this study are shown in Fig. 1. They were installed outside the AIDA chamber and operated at 296 K. The concentrations of O_3 and NO_2 were measured using the gas monitors $O_3$41M and AS32M (both Environment S.A.), respectively.

The concentrations of BCP and low-oxygenated gaseous oxidation products were measured by a Proton-Transfer-Reaction-Time-of-Flight-Mass-Spectrometer (PTR-ToF-MS 4000, Ionicon Analytic GmbH). Data was analysed using PTR viewer 3.3.12. The PTR-ToF-MS is also interfaced with a particle inlet (Chemical Analysis of Aerosol Online, CHARON), which allows to measure the semi-volatile particle components. A detailed description of the CHARON-PTR-MS has been provided elsewhere (Müller et al., 2017; Piel et al., 2021). During the period of BCP injection and ozonolysis, the PTR-ToF-MS was operated for measuring gaseous volatile organic compounds (VOCs) only. After BCP was fully depleted, we switched the PTR-ToF-MS to an alternating measurement mode

for detecting the low-oxygenated organic molecules in both gas and particle phases. This alternating measurement mode included 3-min HEPA filter measurement for the particle background, 5-min CHARON particle measurement, 1-min transition for instrument equilibration, 5-min of VOC measurement and another 1-min

160   transition. The CHARON-PTR-MS measured the particle phase at a sampling flow of 500 SCCM via a 1/4" silcosteel tube, while the gas phase was measured at a flowrate of 100 SCCM via a 1/16" PEEK tube taken from the particle measurement flow. Furthermore, a flowrate of 3.9 l/min was added to the total flow to minimize the residence time in the sampling tube. For measuring gases, the drift tube of the PTR-MS was kept at 393 K and 2.8 mbar leading to an electric field (E/N) of 127 Td. During alternating measurements, the drift tube was

165   automatically optimized to 100 Td for particle measurement. BCP was calibrated using a liquid calibration unit (LCU-a, Ionicon Analytic GmbH). The PTR-ToF-MS at an E/N of 127 Td showed significant fragmentation of BCP, in agreement with previous studies (Kim et al., 2009; Kari et al., 2018). In this study, we observed that the parent ion (m/z 205.20, $C_{15}H_{25}^+$) contributed (29 ± 1) % to total signals of BCP-related ions including m/z 81.07, m/z 95.09, m/z 109.10, m/z 121.10, m/z 137.13, m/z 149.13 and m/z 205.20 (Fig. S1). Therefore, we scaled the

170   concentration of m/z 205.20 ($C_{15}H_{25}^+$) by a factor of 3.45 for the quantification of BCP. The total uncertainty of BCP quantification was estimated as ±20% by including all errors mainly related to the uncertainties of the LCU and the fragmentation pattern of BCP.

Particle size distributions and number concentrations were measured by a scanning mobility particle sizer (SMPS) utilizing a differential mobility analyzer (DMA, 3071 TSI Inc.) connected to a CPC (3772, TSI Inc.). Particle

175   number concentrations were measured by two condensation particle counters (3022a and 3776, TSI Inc.). The particle number size distributions of the SMPS were corrected for the total number concentration measured by a calibrated CPC and used to calculate the SOA mass concentration by applying an effective particle density. This particle density was determined by comparing the mobility and aerodynamic size distributions measured by SMPS and AMS, calculated increasing from 0.9±0.1 at 243K to 1.1 ± 0.1 at 313K, respectively (Saathoff et al., 2009).

180   A High Resolution-Time-of-Flight-Aerosol Mass Spectrometer (HR-ToF-AMS, Aerodyne Inc.) was used to continuously measure the total organic particle mass with a time resolution of 30 seconds at a total flow rate of 0.0011 m³/min (with only 0.0008 m³/min going into the instrument). The data was analyzed using the PIKA v1.60C software. For calculation of the organic particle concentration from the AMS mass spectra, a collection efficiency of 0.6 (determined by comparison with the SMPS results) and an ionization efficiency of 1.52×10^{-7}

185   (calibrated with 300 nm ammonium nitrate particles) were used.

Furthermore, we used a chemical ionization mass spectrometer (CIMS) equipped with a Filter Inlet for Gases and AEROsols (FIGAERO) (Aerodyne Research Inc.) using iodide as the reagent ion to measure both gas-phase and particle-phase components. The FIGAERO-iodide-CIMS has been described in detail by Lopez-Hilfiker et al. (Lopez-Hilfiker et al., 2014). It allows very sensitive detection of oxygenated compounds avoiding significant

190   fragmentation. In our experiments, the gas-phase compounds were measured online by FIGAERO-iodide-CIMS with a total flow rate of 0.005 m³/min, with only 0.002 m³/min going into the instrument. In parallel, particles were deposited offline on prebaked Teflon filters (Polytetrafluoroethylene, PTFE, 1 μm, SKC Inc.) using a stainless-steel filter holder with a flow rate of 0.006 m³/min for 5 min, the same offline sampling procedure as described by Huang et al. (2019a). After particle deposition, the filter samples were stored at 243 K for analysis

195   after the experiment. These filters were then heated by FIGAERO-iodide-CIMS using a flow of ultra-high purity nitrogen as carrier gas following a thermal desorption procedure from 296 K to a maximum temperature of 473

K with a total desorption time of 35 minutes (Huang et al., 2018). The data analysis was done with the Tofware software (version 3.1.2). Note that the reagent ion I- ($m/z = 126.9$) was subtracted from the mass-to-charge ratio of all the molecules shown in this work. For the comparison of measured total particle mass concentration between AMS, SMPS and FIGAERO-iodide-CIMS, we use the maximum sensitivity of 22 cps ppt^{-1} to convert the signals to mass concentration (Lee et al., 2014; Lopez-Hilfiker et al., 2016). In addition, we did a mass calibration for β-caryophyllinic acid (95%, Toronto Research Chemicals) resulting in a sensitivity of ($2.4 \, ^{+0.96}_{-0.63}$) cps ppt^{-1} (details are given in Fig. S2).

Typically, background measurements for both gas and particle phase were done before and after the first addition of BCP to identify any contamination inside the chamber. However, gas background levels were almost negligible for most experiments and most of the particle background signals were from filter matrix contaminations mainly due to fluorinated constituents.

2.3 Rate coefficient calculation

Based on the PTR-MS measurements of the BCP decay as well as the ozone measurements, the rate coefficients of the reaction of BCP with ozone can be determined. As BCP has two double bonds with reactivities with ozone differing by a factor of 100 (Shu and Atkinson, 1994), here we discuss only the rate coefficient for the reaction of the most reactive endocyclic double bond. Since we did not use an OH radical scavenger, the reaction between BCP and OH radicals, which are generated from BCP ozonolysis, was included in our analysis. Employing the following reaction scheme, the observed decays of ozone and BCP were fitted by adjusting only the rate for reaction R1.

$BCP + O_3 \rightarrow$ products $+ \gamma \cdot OH$ (R1)

$BCP + \cdot OH \rightarrow$ products   (R2)
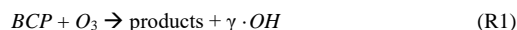
For the reaction of OH radicals with BCP, the rate coefficient of $(1.97\pm0.25)\times10^{-10}$ cm^3 molecule^{-1} determined for 296 K (Shu and Atkinson, 1995; Winterhalter et al., 2009) was used for all temperatures due to the lack of its temperature dependence.

To integrate this simple model and to fit the rate coefficient for reaction R1 we used the software KinSim (Kinetics Simulator for Chemical-Kinetics and Environmental-Chemistry Teaching, version 4.14) (Peng and Jimenez, 2019). The OH radical yields (γ in R1) varied between 5-15% at different temperatures (see section 3.1).

2.4 SOA yields calculation

The SOA yields (Y_{SOA}) were calculated as $Y_{SOA}=\Delta M_{org}/\Delta VOC$, where ΔM_{org} is the SOA mass formed from the reacted mass of BCP (ΔVOC). Similarly, the yields (Y_{BCA}) of BCA, the typical product of BCP ozonolysis, were calculated as $Y_{BCA}= \Delta M_{BCA}/\Delta VOC$, where ΔM_{BCA} is the mass concentration of β-caryophyllinic acid formed from the reacted mass of BCP (ΔVOC). We used a more than 5-fold ozone excess in this study for all temperatures to facilitate oxidation of all double bonds in BCP and its oxidation products. This should lead to more comparable yields for all conditions studied (Li et al., 2011; Chen et al., 2012). Wall losses of particles and semi volatile trace gases were calculated with the aerosol dynamic model COSIMA (Naumann, 2003; Saathoff et al., 2009) and used to correct the yields. The yields were calculated for the initial period of the experiments, which lasted about 90 minutes. During this relatively short time period and due to the large size of the simulation chamber, particle

235   losses contributed typically 6% or less to the total SOA mass. Due to the relatively small particle sizes at the beginning of the experiments, diffusional losses dominated.

3 Results and discussion

In this chapter we discuss the typical course of the experiments, the kinetics of the reaction of BCP with ozone, the SOA mass yields, as well as the SOA chemical composition in absence and in presence of nitrogen oxides.

3.1 Overview of the experiments and kinetics of BCP ozonolysis

240   Figure 2 shows the evolution of trace gases as well as particle mass and size distribution for BCP ozonolysis at 298K first without and then in presence of nitrogen oxides in experiment 4a and 4b. The time point when ozone was firstly added is regarded as the start of each experiment and is set to zero. As shown in Fig. 2, following the nucleation, the particle size increased to 36 nm and grew further to 57 nm and 69 nm after subsequent additions of ozone and BCP, and finally to 122 nm after NO_2 addition. The particle mass increased in presence of the low

245   initial ozone concentration (25 ppb) and stabilized within 20 minutes after increasing the ozone level to above 300 ppb reaching 13.3 $\mu g\ m^{-3}$. A second addition of more BCP led to another increase of the particle mass stabilizing at a level of 17.0 $\mu g\ m^{-3}$. To this SOA, 42 ppb of NO_2 were added, which reacted with the excess of ozone forming NO_3 radicals and consequently led to a small increase in particle size and mass (1.9 nm and 0.9 $\mu g\ m^{-3}$, respectively) due to their reaction with BCP oxidation products. After the third addition of BCP to the reaction mixture, the

250   SOA mass concentration increased to 50.6 $\mu g\ m^{-3}$. For the other four temperatures, these values are given in Table 1. During the final addition of BCP, the existing particles grew quickly and new particle formation were observed. The discrepancy in mass concentrations obtained from SMPS and HR-TOF-AMS in the initial phase of the experiment are due to the fact that smaller particles are poorly detected by the HR-TOF-AMS due to the lower transmission of sub-100nm particles in the aerodynamic lens (Liu et al., 2007; Williams et al., 2013). After 160

255   minutes, the particle size reached 122 nm and both mass concentrations agreed well assuming a collection efficiency of 0.6 for the AMS. Please note that the FIGAERO-iodide-CIMS is sensitive to more polar oxidized compounds, thus, the sum of all compounds detected by CIMS can only be a fraction of the total organic aerosol compounds measured by HR-TOF-AMS. On average 36-61 % of the total organic mass concentration was detected by FIGAERO-iodide-CIMS.

260   After the first addition of an excess of ozone, BCP was depleted within less than 5 minutes. An example of the kinetic model results for the experiment at 313 K is compared to the measured data in Fig. S3 and all kinetic parameters fitted are listed in Table S2. The OH radical yields from the ozonolysis reaction increase from (5±2) % at 243 K to (15±2) % at 313K, and 91-92% of the BCP are calculated to react with ozone under 243-313K.

  Figure 3 shows the temperature dependence of the rate coefficients for BCP ozonolysis. The rate coefficient we

265   determined for 298 K of $(1.09\pm0.21) \times 10^{-14}\ cm^3\ molecule^{-1}\ s^{-1}$ agrees very well with values from Shu and Atkinson (1994) of $(1.16 \pm 0.43) \times 10^{-14}\ cm^3\ molecule^{-1}\ s^{-1}$ and Richters et al. (2015) of $(1.1\pm 0.3) \times 10^{-14}\ cm^3\ molecule^{-1}\ s^{-1}$ for 296 K. At lower temperatures, the rate coefficient increases. This is in an agreement with the density-functional theory (DFT) quantum chemical calculations by Nguyen et al. (2009) but with a slightly higher slope. The Arrhenius equation fitted to our measured values is $k = (1.6\pm0.4) \times10^{-15} \times exp((559\pm97)/T)$. This corresponds

270   to a reaction enthalpy of (5.6±1.0) KJ mol^{-1} in our analysis. Please note that the experiment at 273 K was not used for this analysis because of an unusual background signal in the PTR-MS measurement (Fig. S5b).

3.2 Particle mass yields

Figure 4 presents the yields from BCP ozonolysis in the absence of NO_2 as a function of the temperature for a constant total organic particle mass concentration (M_{org}) of 10 µg m^{-3}. The SOA yields decrease with increasing

275   temperatures from 243K to 313K. For this organic particle mass concentration, we determined a SOA yield of (19.4±6) % at 298K, which was lower by around 55% and 40% than those reported by Chen et al., (2012) and Tasoglou and Pandis (2015), respectively, for a similar particle mass. However, the results are still within the combined uncertainty limits. Please note that these two previous studies used OH radical scavengers, which should lead to lower yields, since OH radicals may oxidize potentially more VOCs causing higher SOA yields. The

280   temperature dependence we observed is significantly lower than e.g. for α-pinene (Saathoff et al., 2009) and hence reflects the generally lower vapour pressure of the condensable oxidation products compared to the monoterpene. In our study, the SOA formation time of about 90 minutes was longer than the typical lifetime of the first-generation products from BCP ozonolysis (20 minutes) at an ozone level of 300 ppb, thus the difference cannot be explained by potential incomplete reactions. Different initial ozone levels may also contribute to the higher

285   yields reported by Chen et al., (2012) and Tasoglou and Pandis (2015).

An overview of the SOA yields determined by Lee et al., 2006, Winterhalter et al, 2009, Chen et al., 2012 and Tasoglou and Pandis (2015) is given in Fig. S4 in comparison with our results in the temperature range between 243 and 313 K. The SOA masses formed reflect the different oxidation products of differing volatilities (Chan et al., 2007) formed at low and high temperatures, which will be discussed in the following section.

290   **3.3 Chemical characterization of SOA from BCP ozonolysis without nitrogen oxides**

In this section the gas and particle phase molecular composition will be discussed mainly based on the FIGAERO-iodide-CIMS mass spectra, complemented by the CHARON-PTR-MS.

3.3.1 Composition of the gas-phase products

Figure 5 shows the averaged gas-phase mass spectra for all five temperatures in the range 213-313 K, before

295   adding NO_2 and when the SOA concentration was in a relatively stable state. Only compounds with mass-to-charge ratios less than 400 Th contributed significantly to the FIGAERO-iodide-CIMS spectra. The signals were normalized to the total gas-phase $C_xH_yO_z$ compounds at each temperature. In the temperature range of 213 – 273 K, $C_{15}H_{24}O_3$ (likely β-caryophyllonic acid), $C_{15}H_{24}O_4$ (likely β-hydroxycaryophyllonic acid), $C_{15}H_{26}O_4$ (not identified yet), $C_{14}H_{22}O_4$ (β-nocaryophyllonic acid or β-caryophyllinic acid) were the most dominant monomeric

300   compounds in the gas phase. These compounds have been identified as products from BCP ozonolysis at room temperature in previous studies (Jaoui et al., 2003; Winterhalter et al., 2009; Chan et al., 2011; Li et al., 2011). In addition, we also observed several abundant ions, such as $C_{14}H_{20}O_2$, $C_{15}H_{22}O_2$ and $C_{14}H_{20}O_3$, in the PTR-MS mass spectra (Fig. S5). As mentioned above, the PTR-MS is more sensitive to less-oxygenated organic compounds and is prone to fragmentation via e.g. losing H_2O. In combination with FIGAERO-iodide-CIMS data, it is reasonable

305   to interpret that $C_{15}H_{22}O_2$ in PTR-MS mass spectra is most likely the fragmentation ion from $C_{15}H_{24}O_3$ via losing H_2O. Besides, $C_{15}H_{24}O_2$ and its potential fragmentation ion $C_{15}H_{22}O$ could be tentatively identified as BCP

aldehyde based on previous studies (Li et al., 2011). This indicates that the low oxidized monomeric compounds (O<5), which are abundant at lower temperatures, can also be formed at higher temperatures (273-313K) but react (cf. Fig. S7) to form higher oxygenated and lower volatile compounds. It cannot be excluded that low molecular-

310 weight compounds, like $C_4H_6O_4$ and $C_2H_4O_3$, might be from the similar process.

3.3.2 Composition of the particle-phase products

Figure 6 shows the particle-phase mass spectra from BCP ozonolysis for 213 K and 313 K. For both lowest and highest temperatures, several first- and second-generation oxidation products, some of which have been identified also in previous studies, were observed, e.g. $C_{14}H_{22}O_4$ (β-caryophyllinic acid or β-hydroxynocaryophyllon

315 aldehyde), $C_{15}H_{24}O_3$ (β-hydroxycaryophyllon aldehyde or β-caryophyllonic acid), and $C_{14}H_{22}O_7$ (2,3-dihydroxy-4-[2-(4-hydroxy-3-oxobutyl)-3,3-dimethylcyclobutyl]-4-oxobutanoic acid) (Jaoui et al., 2007; Li et al., 2011; Winterhalter et al., 2009; Chan et al., 2011; Jaoui et al., 2003; Griffin et al., 1999; Lee et al., 2006a; Lee et al., 2006b; Nguyen et al., 2009; Jenkin et al., 2012; Richters et al., 2016). Table S3 lists all major particulate $C_xH_yO_z$ compounds detected by FIGAERO-iodide-CIMS in this work. Furthermore, we also observed e.g., $C_{14}H_{20}O_2$ H^+,

320 $C_{14}H_{20}O_3$ H^+, $C_{14}H_{22}O_3$ H^+, $C_{15}H_{22}O_2$ H^+ and $C_{15}H_{22}O_3$ H^+ with the CHARON-PTR-MS (Fig. S6). From previous studies we know that CHARON-PTR-MS measurements are affected by fragmentation, e.g. by losing H_2O, CO and CO_2, due to the relatively high collisional energy in the drift tube (100-170 Td) (Gkatzelis et al., 2018). In this study, we operated the CHARON-PTR-MS at 100 Td for the particle measurement. Taking fragmentation by losing one H_2O into account, it is reasonable to speculate that $C_{14}H_{20}O_3$ and $C_{15}H_{22}O_2$ are from the fragmentation

325 of $C_{14}H_{22}O_4$ and $C_{15}H_{24}O_3$, respectively. Similarly, $C_{14}H_{20}O_2$ and $C_{15}H_{22}O_3$ in CHARON-PTR-MS mass spectra could be identified as the fragmentation ions from $C_{14}H_{22}O_3$ and $C_{15}H_{24}O_4$, respectively, which were the most abundant ions in the FIGAERO-iodide-CIMS mass spectra as shown in Fig. 6.

At 213 K, monomers, dimers and trimers are clearly visible. The most abundant compounds measurable with our FIGAERO-iodide-CIMS in each group are $C_{15}H_{24}O_3$, $C_{30}H_{48}O_5$ and $C_{44}H_{68}O_9$, respectively. At 313 K, the

330 monomers dominate and only a few dimers are observed, with the most abundant signals by compounds $C_{14}H_{22}O_7$ and $C_{29}H_{44}O_{10}$, respectively.

Compared to 213K, it is evident that the monomeric compounds formed at 313K are more oxygenated and have higher elemental O:C ratios (Fig. 6). It is inferred that at higher temperatures, once the first-generation products are formed in the gas phase, some of them can remain in the gas due to higher saturation vapor pressures. and

335 undergo further oxidation reactions of their unsaturated exocyclic double bonds with the excess of ozone. Since the saturation vapor pressures of the compounds at 213K are substantially lower than at 313K, more relatively lower oxidized molecules are found in the particle phase due to rapid condensation. For the compounds remaining in the gas phase, HOMs such as e.g. $C_{14}H_{22}O_7$ could be formed via simple or extended autoxidation (Richters et al. (2016)). In addition to $C_{14}H_{22}O_7$, we also detected several other compounds (e.g. $C_{14}H_{22}O_9$, $C_{15}H_{22}O_{7,9}$, and

340 $C_{15}H_{24}O_{7,9}$) that are likely products of autoxidation reactions (Jokinen et al., 2016). At 313K, the monomeric highly oxidized compounds (MHOC, C≤15, O≥6) dominate the monomers with a signal fraction of 42.5% to total organic signals, which exceeds the contribution of other monomeric low oxygenated organic compounds (MLOC, C≤15, O<6) with a signal fraction of 24.9%. For comparison, at 213K, MHOC and MLOC contribute 6.9% and 30.5%, respectively. Furthermore, the six confirmed HOM have signal fractions of 9.2% at 313K and nearly zero

345 at 213K. Note that higher oxygenated autoxidation products like $C_{15}H_{22}O_{11}$ (detected by Atmospheric Pressure

interface Time-Of-Flight mass spectrometer (CI-APi-TOF) using nitrate as the reagent ion (Jokinen et al., 2016)) and $C_{15}H_{22}O_{13}$ could not be detected in this work due to instrument limitations (Riva et al., 2019). To summarize, the relative abundance of HOMs were higher at increasing temperatures (Fig. 8), indicating that the autoxidation showed a strong temperature dependence, slowing down at reduced temperatures.

350   The dimer groups show two completely different patterns at 213K and 313K. At 213K, the dimers mainly consist of low oxygenated organic compounds (DLOC) with 28-30 carbon atoms and 5-8 oxygen atoms, and the total signal fraction of the dimeric compounds is 53.7%. At 313K, dimers are more oxygenated with 9-11 oxygen atoms with the same carbon number of 28-30 (DHOC), and they contribute less to the total normalised organic signal (27.6%). Here, we put forward esterification as a potential pathway for forming the most abundant dimers at both

355   213K and 313K, similar to the dimer formation of other biogenic VOCs suggested by Yasmeen et al. (2010) and Müller et al. (2008). The dominating dimeric molecule at 213K, $C_{30}H_{48}O_5$, could potentially be formed via esterification of two of the most abundant monomers ($C_{15}H_{26}O_3$ and $C_{15}H_{24}O_3$). In a similar way, the dimer $C_{29}H_{44}O_9$ could be formed at 313K from $C_{14}H_{22}O_7$ and $C_{15}H_{24}O_3$. These reactions are described in Fig. S8 in the supplement.

360   However, we cannot exclude the reaction of a BCP-derived stabilized Criegee intermediate and an abundant acid as a potential pathway for $C_{30}H_{48}O_5$ formation, similar to mechanisms suggested for e.g. α-pinene (Kristensen et al., 2016; Wang et al., 2016; Witkowski and Gierczak, 2014; Lee and Kamens, 2005). The dimers we observed had no more than 11 oxygen atoms, which is due to low sensitivities of FIGAERO-iodide-CIMS to these compounds (Riva et al., 2019).

365   Significant signals of trimers at 213K are assigned to $C_{41-43}H_{62-68}O_{9-11}$, but they are not detected at 313K. The potential formation pathway of $C_{44}H_{68}O_9$ at 213K is also included in Fig. S8. Please note, that the assignment for ions at mass to charge ratios of more than 700 Th has significantly higher uncertainties as for smaller mass peaks. Figure 7 presents the averaged mass spectra of SOA particles formed from BCP ozonolysis before NO_2 addition at all five temperatures. With increasing temperature, the most abundant monomeric compounds shift to higher

370   masses with higher elemental O:C ratios, e.g. from $C_{15}H_{24}O_3$ (m/z = 252.2, O:C = 0.20, 213-243K), $C_{15}H_{24}O_4$ (m/z = 268.2, O:C = 0.27, 273K) to $C_{14}H_{22}O_6$ (m/z = 286.1, O:C = 0.43, 298K) and $C_{14}H_{22}O_7$ (m/z = 302.1, O:C = 0.5, 313K). This indicates again that at higher temperatures, after ozonolysis of the endocyclic bond (formation of first-generation oxidation products), the unsaturated compounds can react further with the excess of ozone and form higher oxidized products (e.g. HOM), while those formed at lower temperatures would partition into the

375   condensed phase before further oxidation can occur. As shown in Fig. 8, the monomer groups (MHOC+MLOC) contribute 39.2%, 64.7%, 85.3%, 68.9% and 67.5% to the total signal from 213K to 313K, respectively. Among all the monomers, the signal fraction of the six identified HOM to the total signals of all organic species has a monotonic positive temperature dependence (cf. Fig. 8), increasing from 0.1% to 9.2% for temperatures increasing from 213K to 313K. This is a similar correlation between HOM formation and temperatures as observed by

380   (Bianchi et al., 2019).

Two different dimeric patterns appear in the temperature range of 213-313K. One pattern is represented by molecular formulae of $C_{28-30}H_{42-48}O_{5-8}$ at 213-243K (marked as low temperature group, LT-group), and the other pattern is represented by $C_{28-30}H_{36-44}O_{9-11}$ at 273-313K (marked as high temperature group, HT-group). The LT-group contributes 53.7% at 213K and 32.8% at 243K, with a negative temperature dependence, while the dimeric

385   signal fraction of the HT-group is lower than LT-group, contributing 13.8% at 273K, 24.6% at 298K, and 27.6%

at 313K, respectively, as shown in Fig. 8. After 273K, dimer formation is enhanced with increasing temperatures. The contribution in gas and particle phase of the major compounds are shown in Fig. S9.

3.4 Chemical characterization of SOA from BCP ozonolysis in presence of nitrogen oxides

In this section we discuss the chemical composition of SOA from BCP ozonolysis in the presence of nitrogen

390 oxides including NO_3 radicals, which refers to the SOA formed after the last addition of BCP, e.g. 180-190 min in Fig. 2. Please note that the results given here refer to the total SOA which was formed in two steps, first by pure ozonolysis and in a subsequent step including nitrogen oxides. The SOA mass formed in the presence of nitrogen oxides compared to the total SOA mass detected corresponds to 49% at 213K, 34% at 243K, 49% at 273K, 65% at 298K, and 63 % at 313K. Due to the excess of ozone besides NO_2, also NO_3 radicals and N_2O_5

395 were present. Thus, the BCP was now also oxidized by reaction with NO_3 radicals, with a major pathway to produce organonitrates (org-Ns) (Kiendler-Scharr et al., 2016; Wu et al., 2021). The concentrations of NO_3 radicals before the final addition of BCP were estimated for each experiment using a kinetic box model (details in Fig. S10) and the results are given in Table 1.

Based on the ozone and NO_3 concentration levels as well as the corresponding reaction rates, we estimated the

400 fraction of NO_3 radicals contributing to the initial BCP oxidation to 84%, 90% and 72% for 273, 298 and 313K.

3.4.1 Mass spectra from the gas-phase products

Figure 9 shows the averaged gas-phase mass spectra including molecules without nitrogen atom (org) and organonitrates (org-Ns) for all temperatures as detected by CIMS after the particle concentration got stable after the last BCP addition (e.g., at 298K, referring to the time period after 160 min in Fig. 2). The gas phase

405 organonitrates showed an abundance increasing with temperature from 20.7% at 213K, 26.0% at 243K, 38.3% at 273K, 46.5% at 298K, to 48.9% at 313K. These compounds consisted of three groups of different carbon numbers ($C_5H_7O_6N$, $C_{10}H_{15}O_{5-7}N$ and $C_{15}H_{23,25}O_{6-8}N$). To illustrate more clearly the organonitrate formation, we show the time evolution of the three most abundant org-Ns in these three groups in the right panel of Fig. 9. The signals of $C_5H_7O_6N$ and $C_{10}H_{15}O_6N$ increased after the NO_2 addition immediately, indicating that their formation was related

410 to reactions between BCP oxidation products (BCP+O_3) and NO_3 radicals. After the start of the last BCP addition, $C_{15}H_{25}O_7N$ started to increase significantly, indicating that its formation was linked to the reaction of BCP and NO_3 directly, but not the reaction between the nitrate radicals and oxidation products from BCP ozonolysis.

3.4.2 Mass spectra from the particle phase

Figure 10 shows the particle chemical composition of SOA from BCP ozonolysis in the presence of NO_2 at 213

415 K (upper panel) and 313 K (lower panel). At 213K (upper panel), org dominated the particle composition, with a signal fraction of 97.1% to total signals (org-Ns + org), similar to the SOA before NO_2 addition at 213K. Org groups of monomers (41.2% in signal fraction), dimers (48.2%) and trimers (7.4%) were observed. The most abundant signals in each group were $C_{15}H_{24}O_3$, $C_{30}H_{48}O_5$ and $C_{44}H_{68}O_9$, respectively. The largest org-Ns signal was from $C_{15}H_{25}O_7N$, contributing 0.6% to the total signals. It is obvious that only few org-Ns were formed at

420 213K in our study, with a contribution ([org-Ns]/[total org.]) of 2.8% measured by FIGAERO-iodide-CIMS (normalised signal fraction, Fig. 12) and 0.08 detected by HR-AMS (Fig. S11).

Compared to the SOA chemical composition at 213K, substantially more org-Ns (48.9% to total signals) were formed at 313K. Monomeric org-Ns ($C_{15}H_{23,25}O_{6-10}N$) made up 35.5% of total signal (and the AMS measured 61% of org-Ns to total mass concentration of organic components (Fig. S11)). The most abundant monomeric org-Ns

425   signals at 313K were $C_{15}H_{23-25}O_{7-9}N$, which had also been detected by (Wu et al., 2021). In our study, 51.1% of normalised signals were contributed by org species, with 28.3% of monomeric org ($C_{13-15}H_{20-24}O_{4-8}$), 16.6% of dimeric org ($C_{20}H_{22-24}O_{7-9}$) and 6.3% of trimeric org ($C_{35}H_{48}O_{10-13}$).

The particle mass spectra for all temperatures are shown in Fig. 11, with relative signal abundance of individual molecule to total detected species, including pure organic components (org, red) and organonitrates (org-Ns, blue).

430   Among all the org, the most abundant signal at 298-313K was not $C_{14}H_{22}O_7$ as for pure ozonolysis, but $C_{15}H_{24}O_4$ (NO_3 present), due to the additional formation of pure MLOCs. This could be confirmed by comparison of the absolute signals of $C_{14}H_{22}O_7$ and $C_{15}H_{24}O_4$ in the particles before and after the last BCP addition (Fig. S12). Moreover, the dimeric compounds with 20 carbon atom skeletons (i.e. $C_{20}H_{24}O_{7-8}$, insertion in Fig. 10) and the trimeric compounds with 35 carbon atom skeletons (i.e. $C_{35}H_{48}O_{12}$, Fig. 10 and Fig. 11) were newly formed at

435   higher temperatures (> 273K) in the presence of nitrogen oxides. However, it cannot be excluded that they could be formed by reaction of the oxidation products from BCP ozonolysis (nitrogen oxides absent) and the next step (nitrogen oxides present). In contrast, the mass spectra of non-N-containing organic species (org) at 213-243K showed no substantial changes compared to the species from ozonolysis without nitrogen oxides present (cf. Fig. 7). One obvious reason for this is the lower NO_3 radical concentration at lower temperatures but also changes in

440   the active reaction pathways may play a role.

In addition, more organonitrates were detected at increased temperatures, ranging from 2.8% (213K) to 51.5% (298K) and 48.9% (313K), dominated by monomeric org-Ns ($C_{15}H_{23,25}O_{6-10}N$), wherein the most abundant signals were from $C_{15}H_{25}O_7N$ at 243-273K and $C_{15}H_{23}O_9N$ at 298-313K. Monomeric organonitrates contributed 1.7% to 40.1% from 213 K to 298K, and 35.5% at 313K to total organic signals, as shown in Fig. 12. Besides, the signal-

445   weighted averaged O:C of organonitrates monotonically increased from 0.41 to 0.51 from 213K to 298K, and 0.50 at 313K. We assume that the positive impact of temperature on the oxygenation and formation of organonitrates could also be relevant for the highest temperature (313K). However, the higher oxidized organonitrates may be out of the detection range of the FIGAERO-iodide-CIMS, resulting in less signal fractions and lower signal-weighted averaged O:C ratios of organonitrates at 313K. This is supported by HR-TOF-AMS

450   measurements (Fig. S11), which show increasing organonitrate fractions from 8% to 61% also for 313 K. On the other hand, a potential thermal instability of some organonitrates may also be an explanation for the weaker increase of their fraction observed for 313K.

It should be noted that the nitrate radical levels were estimated to be higher at higher temperatures (Table 1), which partially explains the increasing organonitrates formation at higher temperatures. The orgnonitrates

455   detected in this study were dominantly with the same carbon atom skeleton (C_{15}) and only one organonitrate functional group (-ONO_2). The O:C ratios for organonitrates increase with temperature. Thus, it can be concluded that higher temperatures favour the formation of higher oxygenated organonitrates from the BCP ozonolysis in the presence of NO_3 radicals. The contribution in gas and particle phase of the major compounds are shown in Fig. S13.

460 **4 Summary and conclusions**

In this work, a series of experiments conducted in the dark AIDA chamber with temperatures covering the whole tropospheric range (213-313K) were analysed to investigate the yields, kinetics and chemistry of BCP ozonolysis in the absence and presence of nitrogen oxides. The rate coefficient of the endocyclic double bond in BCP reacting with ozone was determined in the temperature range between 243 and 313K showing decreasing values with

465 increasing temperature. The rate coefficients agree well with literature data at 296 K and with quantum chemical calculations of the temperature dependence. We determined a reaction enthalpy of (5.6 ± 1.0) KJ mol^{-1} and OH radical yields increasing from (5 ± 2) % at 243K to (15 ± 2) % at 313K.

SOA yields determined for the ozonolysis of BCP show about 50% smaller values than literature data at 298 K, which is still within the combined uncertainty limits. For the first time the temperature dependence of the SOA

470 yield was determined showing values decreasing from (37 ± 11) % to (16 ± 5) % for temperatures increasing from 243 to 313K and a constant organic particle mass of 10 µg m^{-3}. This allows to calculate the potential of BCP to contribute to SOA formation e.g. if reaching higher altitudes in the atmosphere.

The chemical characteristics of BCP pure organic species and organonitrates were determined by the FIGAERO-CIMS using I$^-$ as the reagent ion. Major products and different chemical composition of gas and particle phase

475 with and without NO$_3$ present at all temperatures were resolved. The variation of the ozonolysis temperature revealed substantial impact on the abundance of individual pure organic molecules without nitrogen atoms (org) and organonitrate molecules (org-Ns). In the first generated SOA without nitrogen oxides present, monomers (mainly C$_{14-15}$H$_{22-24}$O$_{3-7}$) and dimers (mainly C$_{28-30}$H$_{44-48}$O$_{5-9}$) were abundant, wherein minor signals of trimers (mainly C$_{41-44}$H$_{62-66}$O$_{9-11}$) were mainly detected at 213K. Potential dimer and trimer formation pathways are

480 proposed. With temperature increasing to 313K, monomers and dimers (C$_{14-15}$H$_{22-24}$O$_{6-9}$ and C$_{27-29}$H$_{42-44}$O$_{9-11}$, respectively) became more oxidized, and no significant trimeric signals were detected.

The positive temperature dependence of the oxygenation of the products was also observed in the BCP organonitrates. In the presence of nitrogen oxides, most of the organonitrates were found as monomers with a C$_{15}$ skeleton with one nitrate group, with their signal-weighted O:C ratio increasing from 0.41 to 0.51 for temperatures

485 in the range between 213K and 313K. Dimeric and trimeric pure organic species without nitrogen atoms (C$_{20}$, C$_{35}$) were newly formed in the presence of nitrogen oxides at 298-313K, which substantially changed the chemical composition of pure organic components and indicates more termination ways might exist.

This work helps to get a better understanding on the yields, kinetics and chemical composition of SOA from BCP ozonolysis over a relatively wide range of temperatures, 213 K to 313 K, which is representative of the real

490 atmosphere from boundary layer to upper troposphere. In addition, SOA volatility is expected to have a strong impact on the SOA formation, and will be discussed in our upcoming paper focusing on the desorption of BCP SOA from filters but also the warming up of the aerosol in the simulation chamber overnight.

Data availability

The data on SOA yields and chemical composition from FIGAERO-iodide-CIMS is accessible at KIT open data

495 (link/DOI, will be completed). Data are available upon request to the corresponding author.

Conflict of interests

The authors declare that they have no conflict of interest.

Author contributions

LG and HS designed the study. Chamber experiments were carried out by LG, HS, JS, FJ and MV. Data analysis
500   and interpretation was performed by LG, HS, CM and WH. LG wrote the manuscript, with input from JS and HS.
All co-authors commented on the manuscript.

Acknowledgement

LG, JS and FJ acknowledge funding by the China Scholarship Council (CSC). This work was supported by the
Helmholtz Association within the project MOSES (Modular Observation Solutions for Earth Systems) and H2020
505   European Research Council (CHAPAs (grant no. 850614). Much Acknowledge also goes to all the technicians in
IMK-AAF in KIT for their support on this work.

References

Agelopoulos, N. G., Chamberlain, K., and Pickett, J. A.: Factors Affecting Volatile Emissions of Intact Potato
Plants, Solanum tuberosum: Variability of Quantities and Stability of Ratios, Journal of Chemical Ecology, 26,
510   497-511, 10.1023/A:1005473825335, 2000.

Alfarra, M., Hamilton, J., Wyche, K., Good, N., Ward, M., Carr, T., Barley, M., Monks, P., Jenkin, M., and Lewis,
A.: The effect of photochemical ageing and initial precursor concentration on the composition and hygroscopic
properties of β-caryophyllene secondary organic aerosol, Atmospheric Chemistry and Physics, 12, 6417-6436,
2012.

515   Andreae, M. O., Afchine, A., Albrecht, R., Holanda, B. A., Artaxo, P., Barbosa, H. M. J., Borrmann, S., Cecchini,
M. A., Costa, A., Dollner, M., Fütterer, D., Järvinen, E., Jurkat, T., Klimach, T., Konemann, T., Knote, C., Krämer,
M., Krisna, T., Machado, L. A. T., Mertes, S., Minikin, A., Pöhlker, C., Pöhlker, M. L., Pöschl, U., Rosenfeld, D.,
Sauer, D., Schlager, H., Schnaiter, M., Schneider, J., Schulz, C., Spanu, A., Sperling, V. B., Voigt, C., Walser, A.,
Wang, J., Weinzierl, B., Wendisch, M., and Ziereis, H.: Aerosol characteristics and particle production in the
520   upper troposphere over the Amazon Basin, Atmos. Chem. Phys., 18, 921-961, 10.5194/acp-18-921-2018, 2018.

Bianchi, F., Kurtén, T., Riva, M., Mohr, C., Rissanen, M. P., Roldin, P., Berndt, T., Crounse, J. D., Wennberg, P.
O., Mentel, T. F., Wildt, J., Junninen, H., Jokinen, T., Kulmala, M., Worsnop, D. R., Thornton, J. A., Donahue,
N., Kjaergaard, H. G., and Ehn, M.: Highly Oxygenated Organic Molecules (HOM) from Gas-Phase Autoxidation
Involving Peroxy Radicals: A Key Contributor to Atmospheric Aerosol, Chemical reviews, 119, 3472-3509,
525   10.1021/acs.chemrev.8b00395, 2019.

Calogirou, A., Larsen, B., and Kotzias, D.: Gas-phase terpene oxidation products: a review, Atmospheric
Environment, 33, 1423-1439, 1999.

Calvert, J. G., Derwent, R. G., Orlando, J. J., Wallington, T. J., and Tyndall, G. S.: Mechanisms of atmospheric oxidation of the alkanes, 2008.

530 Chan, A., Kroll, J., Ng, N., and Seinfeld, J.: Kinetic modeling of secondary organic aerosol formation: effects of particle-and gas-phase reactions of semivolatile products, Atmospheric Chemistry and Physics, 7, 4135-4147, 2007.

Chan, M., Surratt, J., Chan, A., Schilling, K., Offenberg, J., Lewandowski, M., Edney, E., Kleindienst, T., Jaoui, M., and Edgerton, E.: Influence of aerosol acidity on the chemical composition of secondary organic aerosol from
535 β-caryophyllene, Atmospheric Chemistry and Physics, 11, 1735-1751, 2011.

Charnawskas, J. C., Alpert, P. A., Lambe, A. T., Berkemeier, T., O'Brien, R. E., Massoli, P., Onasch, T. B., Shiraiwa, M., Moffet, R. C., and Gilles, M. K.: Condensed-phase biogenic–anthropogenic interactions with implications for cold cloud formation, Faraday discussions, 200, 165-194, 2017.

Chen, Q., Li, Y., McKinney, K., Kuwata, M., and Martin, S.: Particle mass yield from beta-caryophyllene
540 ozonolysis, Atmospheric Chemistry and Physics, 12, 3165-3179, 2012.

Cheng, Y., Ma, Y., and Hu, D.: Tracer-based source apportioning of atmospheric organic carbon and the influence of anthropogenic emissions on secondary organic aerosol formation in Hong Kong, Atmos. Chem. Phys., 21, 10589-10608, 10.5194/acp-21-10589-2021, 2021.

Ciccioli, P., Brancaleoni, E., Frattoni, M., Di Palo, V., Valentini, R., Tirone, G., Seufert, G., Bertin, N., Hansen, U., and Csiky, O.: Emission of reactive terpene compounds from orange orchards and their removal by within-
545 canopy processes, Journal of Geophysical Research: Atmospheres, 104, 8077-8094, 1999.

Clark, C. H., Kacarab, M., Nakao, S., Asa-Awuku, A., Sato, K., and Cocker III, D. R.: Temperature effects on secondary organic aerosol (SOA) from the dark ozonolysis and photo-oxidation of isoprene, Environmental Science & Technology, 50, 5564-5571, 2016.

550 Dekermenjian, M.: FTIR analysis of aerosol formed in the ozone oxidation of sesquiterpenes, Aerosol Science & Technology, 30, 349-363, 1999.

Duhl, T. R., Helmig, D., and Guenther, A.: Sesquiterpene emissions from vegetation: a review, Biogeosciences, 5, 761-777, 10.5194/bg-5-761-2008, 2008.

Fahey, D. W., Gao, R. S., Möhler, O., Saathoff, H., Schiller, C., Ebert, V., Krämer, M., Peter, T., Amarouche, N.,
555 Avallone, L. M., Bauer, R., Bozóki, Z., Christensen, L. E., Davis, S. M., Durry, G., Dyroff, C., Herman, R. L., Hunsmann, S., Khaykin, S. M., Mackrodt, P., Meyer, J., Smith, J. B., Spelten, N., Troy, R. F., Vömel, H., Wagner, S., and Wienhold, F. G.: The AquaVIT-1 intercomparison of atmospheric water vapor measurement techniques, Atmos. Meas. Tech., 7, 3177-3213, 10.5194/amt-7-3177-2014, 2014.

Faiola, C. L., Buchholz, A., Kari, E., Yli-Pirilä, P., Holopainen, J. K., Kivimäenpää, M., Miettinen, P., Worsnop,
560 D. R., Lehtinen, K. E. J., and Guenther, A. B.: Terpene composition complexity controls secondary organic aerosol yields from scots pine volatile emissions, Scientific Reports, 8, 1-13, 2018.

Fehsenfeld, F., Calvert, J., Fall, R., Goldan, P., Guenther, A. B., Hewitt, C. N., Lamb, B., Liu, S., Trainer, M., and Westberg, H.: Emissions of volatile organic compounds from vegetation and the implications for atmospheric chemistry, Global Biogeochemical Cycles, 6, 389-430, 1992.

565   Geron, C. D., and Arnts, R. R.: Seasonal monoterpene and sesquiterpene emissions from Pinus taeda and Pinus virginiana, Atmospheric Environment, 44, 4240-4251, 2010.

Gkatzelis, G. I., Tillmann, R., Hohaus, T., Müller, M., Eichler, P., Xu, K. M., Schlag, P., Schmitt, S. H., Wegener, R., Kaminski, M., Holzinger, R., Wisthaler, A., and Kiendler-Scharr, A.: Comparison of three aerosol chemical characterization techniques utilizing PTR-ToF-MS: a study on freshly formed and aged biogenic SOA, Atmos.
570   Meas. Tech., 11, 1481-1500, 10.5194/amt-11-1481-2018, 2018.

Griffin, R. J., Cocker III, D. R., Flagan, R. C., and Seinfeld, J. H.: Organic aerosol formation from the oxidation of biogenic hydrocarbons, Journal of Geophysical Research: Atmospheres, 104, 3555-3567, 1999.

Grosjean, D., Williams, E. L., Grosjean, E., Andino, J. M., and Seinfeld, J. H.: Atmospheric oxidation of biogenic hydrocarbons: reaction of ozone with. beta.-pinene, D-limonene and trans-caryophyllene, Environmental Science
575   & Technology, 27, 2754-2758, 1993.

Hansen, U., and Seufert, G.: Temperature and light dependence of β-caryophyllene emission rates, Journal of Geophysical Research: Atmospheres, 108, 2003.

Haque, M. M., Kawamura, K., and Kim, Y.: Seasonal variations of biogenic secondary organic aerosol tracers in ambient aerosols from Alaska, Atmospheric Environment, 130, 95-104, 2016.

580   Hu, D., Bian, Q., Li, T. W., Lau, A. K., and Yu, J. Z.: Contributions of isoprene, monoterpenes, β-caryophyllene, and toluene to secondary organic aerosols in Hong Kong during the summer of 2006, Journal of Geophysical Research: Atmospheres, 113, 2008.

Huang, W., Saathoff, H., Pajunoja, A., Shen, X., Naumann, K. H., Wagner, R., Virtanen, A., Leisner, T., and Mohr, C.: α-Pinene secondary organic aerosol at low temperature: chemical composition and implications for
585   particle viscosity, Atmos. Chem. Phys., 18, 2883-2898, 10.5194/acp-18-2883-2018, 2018.

Huang, W., Saathoff, H., Shen, X., Ramisetty, R., Leisner, T., and Mohr, C.: Seasonal characteristics of organic aerosol chemical composition and volatility in Stuttgart, Germany, Atmos. Chem. Phys., 19, 11687-11700, 10.5194/acp-19-11687-2019, 2019a.

Huang, W., Saathoff, H., Shen, X., Ramisetty, R., Leisner, T., and Mohr, C.: Chemical Characterization of Highly
590   Functionalized Organonitrates Contributing to Night-Time Organic Aerosol Mass Loadings and Particle Growth, Environmental Science & Technology, 53, 1165-1174, 10.1021/acs.est.8b05826, 2019b.

Huang, W., Li, H., Sarnela, N., Heikkinen, L., Tham, Y. J., Mikkilä, J., Thomas, S. J., Donahue, N. M., Kulmala, M., and Bianchi, F.: Measurement report: Molecular composition and volatility of gaseous organic compounds in a boreal forest – from volatile organic compounds to highly oxygenated organic molecules, Atmos. Chem. Phys.,
595   21, 8961-8977, 10.5194/acp-21-8961-2021, 2021.

Jaoui, M., Leungsakul, S., and Kamens, R.: Gas and particle products distribution from the reaction of β-caryophyllene with ozone, Journal of Atmospheric Chemistry, 45, 261-287, 2003.

Jaoui, M., Lewandowski, M., Kleindienst, T. E., Offenberg, J. H., and Edney, E. O.: β-caryophyllinic acid: An atmospheric tracer for β-caryophyllene secondary organic aerosol, Geophysical Research Letters, 34, 2007.

600 Jaoui, M., Kleindienst, T. E., Docherty, K. S., Lewandowski, M., and Offenberg, J. H.: Secondary organic aerosol formation from the oxidation of a series of sesquiterpenes: α-cedrene, β-caryophyllene, α-humulene and α-farnesene with O3, OH and NO3 radicals, Environmental Chemistry, 10, 178-193, 2013.

Jardine, K., Yañez Serrano, A., Arneth, A., Abrell, L., Jardine, A., Van Haren, J., Artaxo, P., Rizzo, L. V., Ishida, F. Y., and Karl, T.: Within-canopy sesquiterpene ozonolysis in Amazonia, Journal of Geophysical Research: 605 Atmospheres, 116, 2011.

Jenkin, M., Wyche, K., Evans, C., Carr, T., Monks, P., Alfarra, M., Barley, M., McFiggans, G., Young, J., and Rickard, A.: Development and chamber evaluation of the MCM v3. 2 degradation scheme for β-caryophyllene, Atmospheric Chemistry & Physics Discussions, 12, 2012.

Jokinen, T., Kausiala, O., Garmash, O., Peräkylä, O., Junninen, H., Schobesberger, S., Yan, C., Sipilä, M., and 610 Rissanen, M. P.: Production of highly oxidized organic compounds from ozonolysis of beta-caryophyllene: laboratory and field measurements, Boreal Environment Research, 2016.

Kammer, J., Flaud, P. M., Chazeaubeny, A., Ciuraru, R., Le Menach, K., Geneste, E., Budzinski, H., Bonnefond, J. M., Lamaud, E., Perraudin, E., and Villenave, E.: Biogenic volatile organic compounds (BVOCs) reactivity related to new particle formation (NPF) over the Landes forest, Atmospheric Research, 237, 104869, 615 https://doi.org/10.1016/j.atmosres.2020.104869, 2020.

Kari, E., Miettinen, P., Yli-Pirilä, P., Virtanen, A., and Faiola, C. L.: PTR-ToF-MS product ion distributions and humidity-dependence of biogenic volatile organic compounds, International Journal of Mass Spectrometry, 430, 87-97, https://doi.org/10.1016/j.ijms.2018.05.003, 2018.

Kiendler-Scharr, A., Mensah, A. A., Friese, E., Topping, D., Nemitz, E., Prevot, A. S. H., Äijälä, M., Allan, J., 620 Canonaco, F., Canagaratna, M., Carbone, S., Crippa, M., Dall Osto, M., Day, D. A., De Carlo, P., Di Marco, C. F., Elbern, H., Eriksson, A., Freney, E., Hao, L., Herrmann, H., Hildebrandt, L., Hillamo, R., Jimenez, J. L., Laaksonen, A., McFiggans, G., Mohr, C., O'Dowd, C., Otjes, R., Ovadnevaite, J., Pandis, S. N., Poulain, L., Schlag, P., Sellegri, K., Swietlicki, E., Tiitta, P., Vermeulen, A., Wahner, A., Worsnop, D., and Wu, H.-C.: Ubiquity of organic nitrates from nighttime chemistry in the European submicron aerosol, Geophysical Research 625 Letters, 43, 7735-7744, https://doi.org/10.1002/2016GL069239, 2016.

Kim, S., Karl, T., Helmig, D., Daly, R., Rasmussen, R., and Guenther, A.: Measurement of atmospheric sesquiterpenes by proton transfer reaction-mass spectrometry (PTR-MS), Atmos. Meas. Tech., 2, 99-112, 10.5194/amt-2-99-2009, 2009.

630   Kirkby, J., Duplissy, J., Sengupta, K., Frege, C., Gordon, H., Williamson, C., Heinritzi, M., Simon, M., Yan, C., Almeida, J., Tröstl, J., Nieminen, T., Ortega, I. K., Wagner, R., Adamov, A., Amorim, A., Bernhammer, A.-K., Bianchi, F., Breitenlechner, M., Brilke, S., Chen, X., Craven, J., Dias, A., Ehrhart, S., Flagan, R. C., Franchin, A., Fuchs, C., Guida, R., Hakala, J., Hoyle, C. R., Jokinen, T., Junninen, H., Kangasluoma, J., Kim, J., Krapf, M., Kürten, A., Laaksonen, A., Lehtipalo, K., Makhmutov, V., Mathot, S., Molteni, U., Onnela, A., Peräkylä, O., Piel, F., Petäjä, T., Praplan, A. P., Pringle, K., Rap, A., Richards, N. A. D., Riipinen, I., Rissanen, M. P., Rondo, L.,

635   Sarnela, N., Schobesberger, S., Scott, C. E., Seinfeld, J. H., Sipilä, M., Steiner, G., Stozhkov, Y., Stratmann, F., Tomé, A., Virtanen, A., Vogel, A. L., Wagner, A. C., Wagner, P. E., Weingartner, E., Wimmer, D., Winkler, P. M., Ye, P., Zhang, X., Hansel, A., Dommen, J., Donahue, N. M., Worsnop, D. R., Baltensperger, U., Kulmala, M., Carslaw, K. S., and Curtius, J.: Ion-induced nucleation of pure biogenic particles, Nature, 533, 521-526, 10.1038/nature17953, 2016.

640   Kivimäenpää, M., Babalola, A. B., Joutsensaari, J., and Holopainen, J. K.: Methyl Salicylate and Sesquiterpene Emissions Are Indicative for Aphid Infestation on Scots Pine, Forests, 11, 573, 2020.

Kleist, E., Mentel, T., Andres, S., Bohne, A., Folkers, A., Kiendler-Scharr, A., Rudich, Y., Springer, M., Tillmann, R., and Wildt, J.: Irreversible impacts of heat on the emissions of monoterpenes, sesquiterpenes, phenolic BVOC and green leaf volatiles from several tree species, Biogeosciences, 9, 5111, 2012.

645   Kristensen, K., Watne, Å. K., Hammes, J., Lutz, A., Petäjä, T., Hallquist, M., Bilde, M., and Glasius, M.: High-molecular weight dimer esters are major products in aerosols from α-pinene ozonolysis and the boreal forest, Environmental Science & Technology Letters, 3, 280-285, 2016.

Laothawornkitkul, J., Taylor, J. E., Paul, N. D., and Hewitt, C. N.: Biogenic volatile organic compounds in the Earth system, New Phytologist, 183, 27-51, 2009.

650   Larsen, B., Lahaniati, M., Calogirou, A., and Kotzias, D.: Atmospheric oxidation products of terpenes: A new nomenclature, Chemosphere, 37, 1207-1220, 1998.

Lee, A., Goldstein, A. H., Keywood, M. D., Gao, S., Varutbangkul, V., Bahreini, R., Ng, N. L., Flagan, R. C., and Seinfeld, J. H.: Gas-phase products and secondary aerosol yields from the ozonolysis of ten different terpenes, Journal of Geophysical Research: Atmospheres, 111, 2006a.

655   Lee, A., Goldstein, A. H., Kroll, J. H., Ng, N. L., Varutbangkul, V., Flagan, R. C., and Seinfeld, J. H.: Gas-phase products and secondary aerosol yields from the photooxidation of 16 different terpenes, Journal of Geophysical Research: Atmospheres, 111, 2006b.

Lee, B. H., Lopez-Hilfiker, F. D., Mohr, C., Kurtén, T., Worsnop, D. R., and Thornton, J. A.: An iodide-adduct high-resolution time-of-flight chemical-ionization mass spectrometer: Application to atmospheric inorganic and
660   organic compounds, Environmental science & technology, 48, 6309-6317, 2014.

Lee, S., and Kamens, R. M.: Particle nucleation from the reaction of α-pinene and O3, Atmospheric Environment, 39, 6822-6832, 2005.

Li, S.-J., Yuan, X.-Y., Li, Q., and Feng, Z.-Z.: Inventory and Characteristics of Biogenic Volatile Organic Compounds (BVOCs) for 12 Deciduous Fruit Trees, Huan jing ke xue= Huanjing kexue, 40, 2078-2085, 2019.

665 Li, Y., Chen, Q., Guzman, M., Chan, C. K., and Martin, S.: Second-generation products contribute substantially to the particle-phase organic material produced by [beta]-caryophyllene ozonolysis, Atmospheric Chemistry and Physics, 11, 121, 2011.

Liu, P. S. K., Deng, R., Smith, K. A., Williams, L. R., Jayne, J. T., Canagaratna, M. R., Moore, K., Onasch, T. B., Worsnop, D. R., and Deshler, T.: Transmission Efficiency of an Aerodynamic Focusing Lens System: Comparison

670 of Model Calculations and Laboratory Measurements for the Aerodyne Aerosol Mass Spectrometer, Aerosol Science and Technology, 41, 721-733, 10.1080/02786820701422278, 2007.

Lopez-Hilfiker, F. D., Mohr, C., Ehn, M., Rubach, F., Kleist, E., Wildt, J., Mentel, T. F., Lutz, A., Hallquist, M., Worsnop, D., and Thornton, J. A.: A novel method for online analysis of gas and particle composition: description and evaluation of a Filter Inlet for Gases and AEROsols (FIGAERO), Atmos. Meas. Tech., 7, 983-1001,

675 10.5194/amt-7-983-2014, 2014.

Lopez-Hilfiker, F. D., Iyer, S., Mohr, C., Lee, B. H., D'Ambro, E. L., Kurtén, T., and Thornton, J. A.: Constraining the sensitivity of iodide adduct chemical ionization mass spectrometry to multifunctional organic molecules using the collision limit and thermodynamic stability of iodide ion adducts, Atmos. Meas. Tech., 9, 1505-1512, 10.5194/amt-9-1505-2016, 2016.

680 Matsunaga, S. N., Niwa, S., Mochizuki, T., Tani, A., Kusumoto, D., Utsumi, Y., Enoki, T., and Hiura, T.: Seasonal variation in basal emission rates and composition of mono-and sesquiterpenes emitted from dominant conifers in Japan, Atmospheric Environment, 69, 124-130, 2013.

Mellouki, A., Wallington, T., and Chen, J.: Atmospheric chemistry of oxygenated volatile organic compounds: impacts on air quality and climate, Chemical reviews, 115, 3984-4014, 2015.

685 Möhler, O., Stetzer, O., Schaefers, S., Linke, C., Schnaiter, M., Tiede, R., Saathoff, H., Krämer, M., Mangold, A., Budz, P., Zink, P., Schreiner, J., Mauersberger, K., Haag, W., Kärcher, B., and Schurath, U.: Experimental investigation of homogeneous freezing of sulphuric acid particles in the aerosol chamber AIDA, Atmos. Chem. Phys., 3, 211-223, 10.5194/acp-3-211-2003, 2003.

Müller, L., Reinnig, M. C., Warnke, J., and Hoffmann, T.: Unambiguous identification of esters as oligomers in

690 secondary organic aerosol formed from cyclohexene and cyclohexene/α-pinene ozonolysis, Atmos. Chem. Phys., 8, 1423-1433, 10.5194/acp-8-1423-2008, 2008.

Müller, M., Eichler, P., D'Anna, B., Tan, W., and Wisthaler, A.: Direct Sampling and Analysis of Atmospheric Particulate Organic Matter by Proton-Transfer-Reaction Mass Spectrometry, Analytical Chemistry, 89, 10889-10897, 10.1021/acs.analchem.7b02582, 2017.

695 Naumann, K.-H.: COSIMA—a computer program simulating the dynamics of fractal aerosols, Journal of Aerosol Science, 34, 1371-1397, https://doi.org/10.1016/S0021-8502(03)00367-7, 2003.

Ng, N. L., Chhabra, P. S., Chan, A. W. H., Surratt, J. D., Kroll, J. H., Kwan, A. J., McCabe, D. C., Wennberg, P. O., Sorooshian, A., and Murphy, S. M.: Effect of NO x level on secondary organic aerosol (SOA) formation from the photooxidation of terpenes, 2007.

700 Nguyen, T. L., Winterhalter, R., Moortgat, G., Kanawati, B., Peeters, J., and Vereecken, L.: The gas-phase ozonolysis of β-caryophyllene (C 15 H 24). Part II: A theoretical study, Physical Chemistry Chemical Physics, 11, 4173-4183, 2009.

Odum, J. R., Hoffmann, T., Bowman, F., Collins, D., Flagan, R. C., and Seinfeld, J. H.: Gas/Particle Partitioning and Secondary Organic Aerosol Yields, Environmental Science & Technology, 30, 2580-2585, 705 10.1021/es950943+, 1996.

Parshintsev, J., Nurmi, J., Kilpeläinen, I., Hartonen, K., Kulmala, M., and Riekkola, M.-L.: Preparation of β-caryophyllene oxidation products and their determination in ambient aerosol samples, Analytical and bioanalytical chemistry, 390, 913-919, 2008.

Peng, Z., and Jimenez, J. L.: KinSim: A Research-Grade, User-Friendly, Visual Kinetics Simulator for Chemical-710 Kinetics and Environmental-Chemistry Teaching, in, ACS Publications, 2019.

Piel, F., Müller, M., Winkler, K., Skytte af Sätra, J., and Wisthaler, A.: Introducing the extended volatility range proton-transfer-reaction mass spectrometer (EVR PTR-MS), Atmospheric Measurement Techniques, 14, 1355-1363, 2021.

Richters, S., Herrmann, H., and Berndt, T.: Gas-phase rate coefficients of the reaction of ozone with four 715 sesquiterpenes at 295 ± 2 K, Physical Chemistry Chemical Physics, 17, 11658-11669, 10.1039/C4CP05542J, 2015.

Richters, S., Herrmann, H., and Berndt, T.: Different pathways of the formation of highly oxidized multifunctional organic compounds (HOMs) from the gas-phase ozonolysis of β-caryophyllene, Atmos. Chem. Phys, 16, 9831-9845, 2016.

Riva, M., Rantala, P., Krechmer, J. E., Peräkylä, O., Zhang, Y., Heikkinen, L., Garmash, O., Yan, C., Kulmala, 720 M., Worsnop, D., and Ehn, M.: Evaluating the performance of five different chemical ionization techniques for detecting gaseous oxygenated organic species, Atmos. Meas. Tech., 12, 2403-2421, 10.5194/amt-12-2403-2019, 2019.

Rodriguez-Saona, C., Crafts-Brandner, S. J., ParÉ, P. W., and Henneberry, T. J.: EXOGENOUS METHYL JASMONATE INDUCES VOLATILE EMISSIONS IN COTTON PLANTS, Journal of Chemical Ecology, 27, 725 679-695, 10.1023/A:1010393700918, 2001.

Saathoff, H., Naumann, K., Möhler, O., Jonsson, A., Hallquist, M., Kiendler-Scharr, A., Mentel, T. F., Tillmann, R., and Schurath, U.: Temperature dependence of yields of secondary organic aerosols from the ozonolysis of α-pinene and limonene, Atmos. Chem. Phys, 9, 1551-1577, 2009.

Shrivastava, M., Andreae, M. O., Artaxo, P., Barbosa, H. M. J., Berg, L. K., Brito, J., Ching, J., Easter, R. C., Fan, 730 J., Fast, J. D., Feng, Z., Fuentes, J. D., Glasius, M., Goldstein, A. H., Alves, E. G., Gomes, H., Gu, D., Guenther,

A., Jathar, S. H., Kim, S., Liu, Y., Lou, S., Martin, S. T., McNeill, V. F., Medeiros, A., de Sá, S. S., Shilling, J. E., Springston, S. R., Souza, R. A. F., Thornton, J. A., Isaacman-VanWertz, G., Yee, L. D., Ynoue, R., Zaveri, R. A., Zelenyuk, A., and Zhao, C.: Urban pollution greatly enhances formation of natural aerosols over the Amazon rainforest, Nature Communications, 10, 1046, 10.1038/s41467-019-08909-4, 2019.

735   Shu, Y., and Atkinson, R.: Rate constants for the gas-phase reactions of O3 with a series of terpenes and OH radical formation from the O3 reactions with sesquiterpenes at 296±2 K, International Journal of Chemical Kinetics, 26, 1193-1205, 1994.

Shu, Y., and Atkinson, R.: Atmospheric lifetimes and fates of a series of sesquiterpenes, Journal of Geophysical Research: Atmospheres, 100, 7275-7281, https://doi.org/10.1029/95JD00368, 1995.

740   Stolzenburg, D., Fischer, L., Vogel, A. L., Heinritzi, M., Schervish, M., Simon, M., Wagner, A. C., Dada, L., Ahonen, L. R., Amorim, A., Baccarini, A., Bauer, P. S., Baumgartner, B., Bergen, A., Bianchi, F., Breitenlechner, M., Brilke, S., Buenrostro Mazon, S., Chen, D., Dias, A., Draper, D. C., Duplissy, J., El Haddad, I., Finkenzeller, H., Frege, C., Fuchs, C., Garmash, O., Gordon, H., He, X., Helm, J., Hofbauer, V., Hoyle, C. R., Kim, C., Kirkby, J., Kontkanen, J., Kürten, A., Lampilahti, J., Lawler, M., Lehtipalo, K., Leiminger, M., Mai, H., Mathot, S.,
745   Mentler, B., Molteni, U., Nie, W., Nieminen, T., Nowak, J. B., Ojdanic, A., Onnela, A., Passananti, M., Petäjä, T., Quéléver, L. L. J., Rissanen, M. P., Sarnela, N., Schallhart, S., Tauber, C., Tomé, A., Wagner, R., Wang, M., Weitz, L., Wimmer, D., Xiao, M., Yan, C., Ye, P., Zha, Q., Baltensperger, U., Curtius, J., Dommen, J., Flagan, R. C., Kulmala, M., Smith, J. N., Worsnop, D. R., Hansel, A., Donahue, N. M., and Winkler, P. M.: Rapid growth of organic aerosol nanoparticles over a wide tropospheric temperature range, Proceedings of the National
750   Academy of Sciences, 115, 9122-9127, 10.1073/pnas.1807604115, 2018.

Tarvainen, V., Hakola, H., Hellén, H., Bäck, J., Hari, P., and Kulmala, M.: Temperature and light dependence of the VOC emissions of Scots pine, Atmos. Chem. Phys., 5, 989-998, 10.5194/acp-5-989-2005, 2005.

van Eijck, A., Opatz, T., Taraborrelli, D., Sander, R., and Hoffmann, T.: New tracer compounds for secondary organic aerosol formation from β-caryophyllene oxidation, Atmospheric Environment, 80, 122-130, 2013.

755   Verma, S. K., Kawamura, K., Deshmukh, D. K., Haque, M. M., and Pavuluri, C. M.: Seasonal Characteristics of Biogenic Secondary Organic Aerosols Over Chichijima Island in the Western North Pacific: Impact of Biomass Burning Activity in East Asia, Journal of Geophysical Research: Atmospheres, 126, e2020JD032987, https://doi.org/10.1029/2020JD032987, 2021.

Von Hessberg, C., Von Hessberg, P., Pöschl, U., Bilde, M., Nielsen, O., and Moortgat, G.: Temperature and
760   humidity dependence of secondary organic aerosol yield from the ozonolysis of β-pinene, Atmos. Chem. Phys, 9, 3583-3599, 2009.

Wagner, R., Bunz, H., Linke, C., Möhler, O., Naumann, K.-H., Saathoff, H., Schnaiter, M., and Schurath, U.: Chamber simulations of cloud chemistry: the AIDA Chamber, in: Environmental simulation chambers: application to atmospheric chemical processes, Springer, 67-82, 2006.

765 Wang, M., Yao, L., Zheng, J., Wang, X., Chen, J., Yang, X., Worsnop, D. R., Donahue, N. M., and Wang, L.: Reactions of atmospheric particulate stabilized Criegee intermediates lead to high-molecular-weight aerosol components, Environmental science & technology, 50, 5702-5710, 2016.

Weikl, F., Ghirardo, A., Schnitzler, J.-P., and Pritsch, K.: Sesquiterpene emissions from Alternaria alternata and Fusarium oxysporum: effects of age, nutrient availability, and co-cultivation, Scientific reports, 6, 22152, 2016.

770 Williams, L. R., Gonzalez, L. A., Peck, J., Trimborn, D., McInnis, J., Farrar, M. R., Moore, K. D., Jayne, J. T., Robinson, W. A., Lewis, D. K., Onasch, T. B., Canagaratna, M. R., Trimborn, A., Timko, M. T., Magoon, G., Deng, R., Tang, D., de la Rosa Blanco, E., Prévôt, A. S. H., Smith, K. A., and Worsnop, D. R.: Characterization of an aerodynamic lens for transmitting particles greater than 1 micrometer in diameter into the Aerodyne aerosol mass spectrometer, Atmos. Meas. Tech., 6, 3271-3280, 10.5194/amt-6-3271-2013, 2013.

775 Winterhalter, R., Herrmann, F., Kanawati, B., Nguyen, T. L., Peeters, J., Vereecken, L., and Moortgat, G. K.: The gas-phase ozonolysis of β-caryophyllene (C 15 H 24). Part I: an experimental study, Physical Chemistry Chemical Physics, 11, 4152-4172, 2009.

Witkowski, B., and Gierczak, T.: Early stage composition of SOA produced by α-pinene/ozone reaction: α-Acyloxyhydroperoxy aldehydes and acidic dimers, Atmospheric Environment, 95, 59-70, 2014.

780 Wu, C., Bell, D. M., Graham, E. L., Haslett, S., Riipinen, I., Baltensperger, U., Bertrand, A., Giannoukos, S., Schoonbaert, J., El Haddad, I., Prevot, A. S. H., Huang, W., and Mohr, C.: Photolytically induced changes in composition and volatility of biogenic secondary organic aerosol from nitrate radical oxidation during night-to-day transition, Atmos. Chem. Phys., 21, 14907-14925, 10.5194/acp-21-14907-2021, 2021.

Yasmeen, F., Vermeylen, R., Szmigielski, R., Iinuma, Y., Böge, O., Herrmann, H., Maenhaut, W., and Claeys,
785 M.: Terpenylic acid and related compounds: precursors for dimers in secondary organic aerosol from the ozonolysis of α- and β-pinene, Atmos. Chem. Phys., 10, 9383-9392, 10.5194/acp-10-9383-2010, 2010.

Ye, Q., Wang, M., Hofbauer, V., Stolzenburg, D., Chen, D., Schervish, M., Vogel, A., Mauldin, R. L., Baalbaki, R., Brilke, S., Dada, L., Dias, A., Duplissy, J., El Haddad, I., Finkenzeller, H., Fischer, L., He, X., Kim, C., Kürten,
790 A., Lamkaddam, H., Lee, C. P., Lehtipalo, K., Leiminger, M., Manninen, H. E., Marten, R., Mentler, B., Partoll, E., Petäjä, T., Rissanen, M., Schobesberger, S., Schuchmann, S., Simon, M., Tham, Y. J., Vazquez-Pufleau, M., Wagner, A. C., Wang, Y., Wu, Y., Xiao, M., Baltensperger, U., Curtius, J., Flagan, R., Kirkby, J., Kulmala, M., Volkamer, R., Winkler, P. M., Worsnop, D., and Donahue, N. M.: Molecular Composition and Volatility of Nucleated Particles from α-Pinene Oxidation between −50 °C and +25 °C, Environmental Science & Technology,
795 53, 12357-12365, 10.1021/acs.est.9b03265, 2019.

Zhao, Y., Zhang, R., Sun, X., He, M., Wang, H., Zhang, Q., and Ru, M.: Theoretical study on mechanism for O3-initiated atmospheric oxidation reaction of β-caryophyllene, Journal of Molecular Structure: THEOCHEM, 947, 68-75, 2010.

Agelopoulos, N. G., Chamberlain, K., and Pickett, J. A.: Factors Affecting Volatile Emissions of Intact Potato
800   Plants, Solanum tuberosum: Variability of Quantities and Stability of Ratios, Journal of Chemical Ecology, 26,
497-511, 10.1023/A:1005473825335, 2000.

Alfarra, M., Hamilton, J., Wyche, K., Good, N., Ward, M., Carr, T., Barley, M., Monks, P., Jenkin, M., and Lewis,
A.: The effect of photochemical ageing and initial precursor concentration on the composition and hygroscopic
properties of β-caryophyllene secondary organic aerosol, Atmospheric Chemistry and Physics, 12, 6417-6436,
805   2012.

Andreae, M. O., Afchine, A., Albrecht, R., Holanda, B. A., Artaxo, P., Barbosa, H. M. J., Borrmann, S., Cecchini,
M. A., Costa, A., Dollner, M., Fütterer, D., Järvinen, E., Jurkat, T., Klimach, T., Konemann, T., Knote, C., Krämer,
M., Krisna, T., Machado, L. A. T., Mertes, S., Minikin, A., Pöhlker, C., Pöhlker, M. L., Pöschl, U., Rosenfeld, D.,
Sauer, D., Schlager, H., Schnaiter, M., Schneider, J., Schulz, C., Spanu, A., Sperling, V. B., Voigt, C., Walser, A.,
810   Wang, J., Weinzierl, B., Wendisch, M., and Ziereis, H.: Aerosol characteristics and particle production in the
upper troposphere over the Amazon Basin, Atmos. Chem. Phys., 18, 921-961, 10.5194/acp-18-921-2018, 2018.

Bianchi, F., Kurtén, T., Riva, M., Mohr, C., Rissanen, M. P., Roldin, P., Berndt, T., Crounse, J. D., Wennberg, P.
O., Mentel, T. F., Wildt, J., Junninen, H., Jokinen, T., Kulmala, M., Worsnop, D. R., Thornton, J. A., Donahue,
N., Kjaergaard, H. G., and Ehn, M.: Highly Oxygenated Organic Molecules (HOM) from Gas-Phase Autoxidation
815   Involving Peroxy Radicals: A Key Contributor to Atmospheric Aerosol, Chemical reviews, 119, 3472-3509,
10.1021/acs.chemrev.8b00395, 2019.

Calogirou, A., Larsen, B., and Kotzias, D.: Gas-phase terpene oxidation products: a review, Atmospheric
Environment, 33, 1423-1439, 1999.

Calvert, J. G., Derwent, R. G., Orlando, J. J., Wallington, T. J., and Tyndall, G. S.: Mechanisms of atmospheric
820   oxidation of the alkanes, 2008.

Chan, A., Kroll, J., Ng, N., and Seinfeld, J.: Kinetic modeling of secondary organic aerosol formation: effects of
particle-and gas-phase reactions of semivolatile products, Atmospheric Chemistry and Physics, 7, 4135-4147,
2007.

Chan, M., Surratt, J., Chan, A., Schilling, K., Offenberg, J., Lewandowski, M., Edney, E., Kleindienst, T., Jaoui,
825   M., and Edgerton, E.: Influence of aerosol acidity on the chemical composition of secondary organic aerosol from
β-caryophyllene, Atmospheric Chemistry and Physics, 11, 1735-1751, 2011.

Charnawskas, J. C., Alpert, P. A., Lambe, A. T., Berkemeier, T., O'Brien, R. E., Massoli, P., Onasch, T. B.,
Shiraiwa, M., Moffet, R. C., and Gilles, M. K.: Condensed-phase biogenic–anthropogenic interactions with
implications for cold cloud formation, Faraday discussions, 200, 165-194, 2017.

830   Chen, Q., Li, Y., McKinney, K., Kuwata, M., and Martin, S.: Particle mass yield from beta-caryophyllene
ozonolysis, Atmospheric Chemistry and Physics, 12, 3165-3179, 2012.

Cheng, Y., Ma, Y., and Hu, D.: Tracer-based source apportioning of atmospheric organic carbon and the influence of anthropogenic emissions on secondary organic aerosol formation in Hong Kong, Atmos. Chem. Phys., 21, 10589-10608, 10.5194/acp-21-10589-2021, 2021.

835   Ciccioli, P., Brancaleoni, E., Frattoni, M., Di Palo, V., Valentini, R., Tirone, G., Seufert, G., Bertin, N., Hansen, U., and Csiky, O.: Emission of reactive terpene compounds from orange orchards and their removal by within-canopy processes, Journal of Geophysical Research: Atmospheres, 104, 8077-8094, 1999.

Clark, C. H., Kacarab, M., Nakao, S., Asa-Awuku, A., Sato, K., and Cocker III, D. R.: Temperature effects on secondary organic aerosol (SOA) from the dark ozonolysis and photo-oxidation of isoprene, Environmental 840   Science & Technology, 50, 5564-5571, 2016.

Dekermenjian, M.: FTIR analysis of aerosol formed in the ozone oxidation of sesquiterpenes, Aerosol Science & Technology, 30, 349-363, 1999.

Duhl, T. R., Helmig, D., and Guenther, A.: Sesquiterpene emissions from vegetation: a review, Biogeosciences, 5, 761-777, 10.5194/bg-5-761-2008, 2008.

845   Fahey, D. W., Gao, R. S., Möhler, O., Saathoff, H., Schiller, C., Ebert, V., Krämer, M., Peter, T., Amarouche, N., Avallone, L. M., Bauer, R., Bozóki, Z., Christensen, L. E., Davis, S. M., Durry, G., Dyroff, C., Herman, R. L., Hunsmann, S., Khaykin, S. M., Mackrodt, P., Meyer, J., Smith, J. B., Spelten, N., Troy, R. F., Vömel, H., Wagner, S., and Wienhold, F. G.: The AquaVIT-1 intercomparison of atmospheric water vapor measurement techniques, Atmos. Meas. Tech., 7, 3177-3213, 10.5194/amt-7-3177-2014, 2014.

850   Faiola, C. L., Buchholz, A., Kari, E., Yli-Pirilä, P., Holopainen, J. K., Kivimäenpää, M., Miettinen, P., Worsnop, D. R., Lehtinen, K. E. J., and Guenther, A. B.: Terpene composition complexity controls secondary organic aerosol yields from scots pine volatile emissions, Scientific Reports, 8, 1-13, 2018.

Fehsenfeld, F., Calvert, J., Fall, R., Goldan, P., Guenther, A. B., Hewitt, C. N., Lamb, B., Liu, S., Trainer, M., and Westberg, H.: Emissions of volatile organic compounds from vegetation and the implications for atmospheric 855   chemistry, Global Biogeochemical Cycles, 6, 389-430, 1992.

Geron, C. D., and Arnts, R. R.: Seasonal monoterpene and sesquiterpene emissions from Pinus taeda and Pinus virginiana, Atmospheric Environment, 44, 4240-4251, 2010.

Gkatzelis, G. I., Tillmann, R., Hohaus, T., Müller, M., Eichler, P., Xu, K. M., Schlag, P., Schmitt, S. H., Wegener, R., Kaminski, M., Holzinger, R., Wisthaler, A., and Kiendler-Scharr, A.: Comparison of three aerosol chemical 860   characterization techniques utilizing PTR-ToF-MS: a study on freshly formed and aged biogenic SOA, Atmos. Meas. Tech., 11, 1481-1500, 10.5194/amt-11-1481-2018, 2018.

Griffin, R. J., Cocker III, D. R., Flagan, R. C., and Seinfeld, J. H.: Organic aerosol formation from the oxidation of biogenic hydrocarbons, Journal of Geophysical Research: Atmospheres, 104, 3555-3567, 1999.

Grosjean, D., Williams, E. L., Grosjean, E., Andino, J. M., and Seinfeld, J. H.: Atmospheric oxidation of biogenic
865   hydrocarbons: reaction of ozone with. beta.-pinene, D-limonene and trans-caryophyllene, Environmental Science
& Technology, 27, 2754-2758, 1993.

Hansen, U., and Seufert, G.: Temperature and light dependence of β-caryophyllene emission rates, Journal of
Geophysical Research: Atmospheres, 108, 2003.

Haque, M. M., Kawamura, K., and Kim, Y.: Seasonal variations of biogenic secondary organic aerosol tracers in
870   ambient aerosols from Alaska, Atmospheric Environment, 130, 95-104, 2016.

Hu, D., Bian, Q., Li, T. W., Lau, A. K., and Yu, J. Z.: Contributions of isoprene, monoterpenes, β-caryophyllene,
and toluene to secondary organic aerosols in Hong Kong during the summer of 2006, Journal of Geophysical
Research: Atmospheres, 113, 2008.

Huang, W., Saathoff, H., Pajunoja, A., Shen, X., Naumann, K. H., Wagner, R., Virtanen, A., Leisner, T., and
875   Mohr, C.: α-Pinene secondary organic aerosol at low temperature: chemical composition and implications for
particle viscosity, Atmos. Chem. Phys., 18, 2883-2898, 10.5194/acp-18-2883-2018, 2018.

Huang, W., Saathoff, H., Shen, X., Ramisetty, R., Leisner, T., and Mohr, C.: Seasonal characteristics of organic
aerosol chemical composition and volatility in Stuttgart, Germany, Atmos. Chem. Phys., 19, 11687-11700,
10.5194/acp-19-11687-2019, 2019a.

880   Huang, W., Saathoff, H., Shen, X., Ramisetty, R., Leisner, T., and Mohr, C.: Chemical Characterization of Highly
Functionalized Organonitrates Contributing to Night-Time Organic Aerosol Mass Loadings and Particle Growth,
Environmental Science & Technology, 53, 1165-1174, 10.1021/acs.est.8b05826, 2019b.

Huang, W., Li, H., Sarnela, N., Heikkinen, L., Tham, Y. J., Mikkilä, J., Thomas, S. J., Donahue, N. M., Kulmala,
M., and Bianchi, F.: Measurement report: Molecular composition and volatility of gaseous organic compounds in
885   a boreal forest – from volatile organic compounds to highly oxygenated organic molecules, Atmos. Chem. Phys.,
21, 8961-8977, 10.5194/acp-21-8961-2021, 2021.

Jaoui, M., Leungsakul, S., and Kamens, R.: Gas and particle products distribution from the reaction of β-
caryophyllene with ozone, Journal of Atmospheric Chemistry, 45, 261-287, 2003.

Jaoui, M., Lewandowski, M., Kleindienst, T. E., Offenberg, J. H., and Edney, E. O.: β-caryophyllinic acid: An
890   atmospheric tracer for β-caryophyllene secondary organic aerosol, Geophysical Research Letters, 34, 2007.

Jaoui, M., Kleindienst, T. E., Docherty, K. S., Lewandowski, M., and Offenberg, J. H.: Secondary organic aerosol
formation from the oxidation of a series of sesquiterpenes: α-cedrene, β-caryophyllene, α-humulene and α-
farnesene with O3, OH and NO3 radicals, Environmental Chemistry, 10, 178-193, 2013.

Jardine, K., Yañez Serrano, A., Arneth, A., Abrell, L., Jardine, A., Van Haren, J., Artaxo, P., Rizzo, L. V., Ishida,
895   F. Y., and Karl, T.: Within-canopy sesquiterpene ozonolysis in Amazonia, Journal of Geophysical Research:
Atmospheres, 116, 2011.

Jenkin, M., Wyche, K., Evans, C., Carr, T., Monks, P., Alfarra, M., Barley, M., McFiggans, G., Young, J., and Rickard, A.: Development and chamber evaluation of the MCM v3. 2 degradation scheme for β-caryophyllene, Atmospheric Chemistry & Physics Discussions, 12, 2012.

900   Jokinen, T., Kausiala, O., Garmash, O., Peräkylä, O., Junninen, H., Schobesberger, S., Yan, C., Sipilä, M., and Rissanen, M. P.: Production of highly oxidized organic compounds from ozonolysis of beta-caryophyllene: laboratory and field measurements, Boreal Environment Research, 2016.

Kammer, J., Flaud, P. M., Chazeaubeny, A., Ciuraru, R., Le Menach, K., Geneste, E., Budzinski, H., Bonnefond, J. M., Lamaud, E., Perraudin, E., and Villenave, E.: Biogenic volatile organic compounds (BVOCs) reactivity

905   related to new particle formation (NPF) over the Landes forest, Atmospheric Research, 237, 104869, https://doi.org/10.1016/j.atmosres.2020.104869, 2020.

Kari, E., Miettinen, P., Yli-Pirilä, P., Virtanen, A., and Faiola, C. L.: PTR-ToF-MS product ion distributions and humidity-dependence of biogenic volatile organic compounds, International Journal of Mass Spectrometry, 430, 87-97, https://doi.org/10.1016/j.ijms.2018.05.003, 2018.

910   Kiendler-Scharr, A., Mensah, A. A., Friese, E., Topping, D., Nemitz, E., Prevot, A. S. H., Äijälä, M., Allan, J., Canonaco, F., Canagaratna, M., Carbone, S., Crippa, M., Dall Osto, M., Day, D. A., De Carlo, P., Di Marco, C. F., Elbern, H., Eriksson, A., Freney, E., Hao, L., Herrmann, H., Hildebrandt, L., Hillamo, R., Jimenez, J. L., Laaksonen, A., McFiggans, G., Mohr, C., O'Dowd, C., Otjes, R., Ovadnevaite, J., Pandis, S. N., Poulain, L., Schlag, P., Sellegri, K., Swietlicki, E., Tiitta, P., Vermeulen, A., Wahner, A., Worsnop, D., and Wu, H.-C.:

915   Ubiquity of organic nitrates from nighttime chemistry in the European submicron aerosol, Geophysical Research Letters, 43, 7735-7744, https://doi.org/10.1002/2016GL069239, 2016.

Kim, S., Karl, T., Helmig, D., Daly, R., Rasmussen, R., and Guenther, A.: Measurement of atmospheric sesquiterpenes by proton transfer reaction-mass spectrometry (PTR-MS), Atmos. Meas. Tech., 2, 99-112, 10.5194/amt-2-99-2009, 2009.

920   Kirkby, J., Duplissy, J., Sengupta, K., Frege, C., Gordon, H., Williamson, C., Heinritzi, M., Simon, M., Yan, C., Almeida, J., Tröstl, J., Nieminen, T., Ortega, I. K., Wagner, R., Adamov, A., Amorim, A., Bernhammer, A.-K., Bianchi, F., Breitenlechner, M., Brilke, S., Chen, X., Craven, J., Dias, A., Ehrhart, S., Flagan, R. C., Franchin, A., Fuchs, C., Guida, R., Hakala, J., Hoyle, C. R., Jokinen, T., Junninen, H., Kangasluoma, J., Kim, J., Krapf, M., Kürten, A., Laaksonen, A., Lehtipalo, K., Makhmutov, V., Mathot, S., Molteni, U., Onnela, A., Peräkylä, O., Piel,

925   F., Petäjä, T., Praplan, A. P., Pringle, K., Rap, A., Richards, N. A. D., Riipinen, I., Rissanen, M. P., Rondo, L., Sarnela, N., Schobesberger, S., Scott, C. E., Seinfeld, J. H., Sipilä, M., Steiner, G., Stozhkov, Y., Stratmann, F., Tomé, A., Virtanen, A., Vogel, A. L., Wagner, A. C., Wagner, P. E., Weingartner, E., Wimmer, D., Winkler, P. M., Ye, P., Zhang, X., Hansel, A., Dommen, J., Donahue, N. M., Worsnop, D. R., Baltensperger, U., Kulmala, M., Carslaw, K. S., and Curtius, J.: Ion-induced nucleation of pure biogenic particles, Nature, 533, 521-526,

930   10.1038/nature17953, 2016.

Kivimäenpää, M., Babalola, A. B., Joutsensaari, J., and Holopainen, J. K.: Methyl Salicylate and Sesquiterpene Emissions Are Indicative for Aphid Infestation on Scots Pine, Forests, 11, 573, 2020.

Kleist, E., Mentel, T., Andres, S., Bohne, A., Folkers, A., Kiendler-Scharr, A., Rudich, Y., Springer, M., Tillmann, R., and Wildt, J.: Irreversible impacts of heat on the emissions of monoterpenes, sesquiterpenes, phenolic BVOC and green leaf volatiles from several tree species, Biogeosciences, 9, 5111, 2012.

Kristensen, K., Watne, Å. K., Hammes, J., Lutz, A., Petäjä, T., Hallquist, M., Bilde, M., and Glasius, M.: High-molecular weight dimer esters are major products in aerosols from α-pinene ozonolysis and the boreal forest, Environmental Science & Technology Letters, 3, 280-285, 2016.

Laothawornkitkul, J., Taylor, J. E., Paul, N. D., and Hewitt, C. N.: Biogenic volatile organic compounds in the Earth system, New Phytologist, 183, 27-51, 2009.

Larsen, B., Lahaniati, M., Calogirou, A., and Kotzias, D.: Atmospheric oxidation products of terpenes: A new nomenclature, Chemosphere, 37, 1207-1220, 1998.

Lee, A., Goldstein, A. H., Keywood, M. D., Gao, S., Varutbangkul, V., Bahreini, R., Ng, N. L., Flagan, R. C., and Seinfeld, J. H.: Gas-phase products and secondary aerosol yields from the ozonolysis of ten different terpenes, Journal of Geophysical Research: Atmospheres, 111, 2006a.

Lee, A., Goldstein, A. H., Kroll, J. H., Ng, N. L., Varutbangkul, V., Flagan, R. C., and Seinfeld, J. H.: Gas-phase products and secondary aerosol yields from the photooxidation of 16 different terpenes, Journal of Geophysical Research: Atmospheres, 111, 2006b.

Lee, B. H., Lopez-Hilfiker, F. D., Mohr, C., Kurtén, T., Worsnop, D. R., and Thornton, J. A.: An iodide-adduct high-resolution time-of-flight chemical-ionization mass spectrometer: Application to atmospheric inorganic and organic compounds, Environmental science & technology, 48, 6309-6317, 2014.

Lee, S., and Kamens, R. M.: Particle nucleation from the reaction of α-pinene and O3, Atmospheric Environment, 39, 6822-6832, 2005.

Li, S.-J., Yuan, X.-Y., Li, Q., and Feng, Z.-Z.: Inventory and Characteristics of Biogenic Volatile Organic Compounds (BVOCs) for 12 Deciduous Fruit Trees, Huan jing ke xue= Huanjing kexue, 40, 2078-2085, 2019.

Li, Y., Chen, Q., Guzman, M., Chan, C. K., and Martin, S.: Second-generation products contribute substantially to the particle-phase organic material produced by [beta]-caryophyllene ozonolysis, Atmospheric Chemistry and Physics, 11, 121, 2011.

Liu, P. S. K., Deng, R., Smith, K. A., Williams, L. R., Jayne, J. T., Canagaratna, M. R., Moore, K., Onasch, T. B., Worsnop, D. R., and Deshler, T.: Transmission Efficiency of an Aerodynamic Focusing Lens System: Comparison of Model Calculations and Laboratory Measurements for the Aerodyne Aerosol Mass Spectrometer, Aerosol Science and Technology, 41, 721-733, 10.1080/02786820701422278, 2007.

Lopez-Hilfiker, F. D., Mohr, C., Ehn, M., Rubach, F., Kleist, E., Wildt, J., Mentel, T. F., Lutz, A., Hallquist, M., Worsnop, D., and Thornton, J. A.: A novel method for online analysis of gas and particle composition: description and evaluation of a Filter Inlet for Gases and AEROsols (FIGAERO), Atmos. Meas. Tech., 7, 983-1001, 10.5194/amt-7-983-2014, 2014.

Lopez-Hilfiker, F. D., Iyer, S., Mohr, C., Lee, B. H., D'Ambro, E. L., Kurtén, T., and Thornton, J. A.: Constraining the sensitivity of iodide adduct chemical ionization mass spectrometry to multifunctional organic molecules using the collision limit and thermodynamic stability of iodide ion adducts, Atmos. Meas. Tech., 9, 1505-1512, 10.5194/amt-9-1505-2016, 2016.

970

Matsunaga, S. N., Niwa, S., Mochizuki, T., Tani, A., Kusumoto, D., Utsumi, Y., Enoki, T., and Hiura, T.: Seasonal variation in basal emission rates and composition of mono-and sesquiterpenes emitted from dominant conifers in Japan, Atmospheric Environment, 69, 124-130, 2013.

Mellouki, A., Wallington, T., and Chen, J.: Atmospheric chemistry of oxygenated volatile organic compounds: impacts on air quality and climate, Chemical reviews, 115, 3984-4014, 2015.

975

Möhler, O., Stetzer, O., Schaefers, S., Linke, C., Schnaiter, M., Tiede, R., Saathoff, H., Krämer, M., Mangold, A., Budz, P., Zink, P., Schreiner, J., Mauersberger, K., Haag, W., Kärcher, B., and Schurath, U.: Experimental investigation of homogeneous freezing of sulphuric acid particles in the aerosol chamber AIDA, Atmos. Chem. Phys., 3, 211-223, 10.5194/acp-3-211-2003, 2003.

980

Müller, L., Reinnig, M. C., Warnke, J., and Hoffmann, T.: Unambiguous identification of esters as oligomers in secondary organic aerosol formed from cyclohexene and cyclohexene/α-pinene ozonolysis, Atmos. Chem. Phys., 8, 1423-1433, 10.5194/acp-8-1423-2008, 2008.

Müller, M., Eichler, P., D'Anna, B., Tan, W., and Wisthaler, A.: Direct Sampling and Analysis of Atmospheric Particulate Organic Matter by Proton-Transfer-Reaction Mass Spectrometry, Analytical Chemistry, 89, 10889-10897, 10.1021/acs.analchem.7b02582, 2017.

985

Naumann, K.-H.: COSIMA—a computer program simulating the dynamics of fractal aerosols, Journal of Aerosol Science, 34, 1371-1397, https://doi.org/10.1016/S0021-8502(03)00367-7, 2003.

Ng, N. L., Chhabra, P. S., Chan, A. W. H., Surratt, J. D., Kroll, J. H., Kwan, A. J., McCabe, D. C., Wennberg, P. O., Sorooshian, A., and Murphy, S. M.: Effect of NO x level on secondary organic aerosol (SOA) formation from the photooxidation of terpenes, 2007.

990

Nguyen, T. L., Winterhalter, R., Moortgat, G., Kanawati, B., Peeters, J., and Vereecken, L.: The gas-phase ozonolysis of β-caryophyllene (C 15 H 24). Part II: A theoretical study, Physical Chemistry Chemical Physics, 11, 4173-4183, 2009.

Odum, J. R., Hoffmann, T., Bowman, F., Collins, D., Flagan, R. C., and Seinfeld, J. H.: Gas/Particle Partitioning and Secondary Organic Aerosol Yields, Environmental Science & Technology, 30, 2580-2585, 10.1021/es950943+, 1996.

995

Parshintsev, J., Nurmi, J., Kilpeläinen, I., Hartonen, K., Kulmala, M., and Riekkola, M.-L.: Preparation of β-caryophyllene oxidation products and their determination in ambient aerosol samples, Analytical and bioanalytical chemistry, 390, 913-919, 2008.

1000   Peng, Z., and Jimenez, J. L.: KinSim: A Research-Grade, User-Friendly, Visual Kinetics Simulator for Chemical-Kinetics and Environmental-Chemistry Teaching, in, ACS Publications, 2019.

Piel, F., Müller, M., Winkler, K., Skytte af Sätra, J., and Wisthaler, A.: Introducing the extended volatility range proton-transfer-reaction mass spectrometer (EVR PTR-MS), Atmospheric Measurement Techniques, 14, 1355-1363, 2021.

1005   Richters, S., Herrmann, H., and Berndt, T.: Gas-phase rate coefficients of the reaction of ozone with four sesquiterpenes at 295 ± 2 K, Physical Chemistry Chemical Physics, 17, 11658-11669, 10.1039/C4CP05542J, 2015.

Richters, S., Herrmann, H., and Berndt, T.: Different pathways of the formation of highly oxidized multifunctional organic compounds (HOMs) from the gas-phase ozonolysis of β-caryophyllene, Atmos. Chem. Phys, 16, 9831-9845, 2016.

1010   Riva, M., Rantala, P., Krechmer, J. E., Peräkylä, O., Zhang, Y., Heikkinen, L., Garmash, O., Yan, C., Kulmala, M., Worsnop, D., and Ehn, M.: Evaluating the performance of five different chemical ionization techniques for detecting gaseous oxygenated organic species, Atmos. Meas. Tech., 12, 2403-2421, 10.5194/amt-12-2403-2019, 2019.

Rodriguez-Saona, C., Crafts-Brandner, S. J., ParÉ, P. W., and Henneberry, T. J.: EXOGENOUS METHYL
1015   JASMONATE INDUCES VOLATILE EMISSIONS IN COTTON PLANTS, Journal of Chemical Ecology, 27, 679-695, 10.1023/A:1010393700918, 2001.

Saathoff, H., Naumann, K., Möhler, O., Jonsson, A., Hallquist, M., Kiendler-Scharr, A., Mentel, T. F., Tillmann, R., and Schurath, U.: Temperature dependence of yields of secondary organic aerosols from the ozonolysis of α-pinene and limonene, Atmos. Chem. Phys, 9, 1551-1577, 2009.

1020   Shrivastava, M., Andreae, M. O., Artaxo, P., Barbosa, H. M. J., Berg, L. K., Brito, J., Ching, J., Easter, R. C., Fan, J., Fast, J. D., Feng, Z., Fuentes, J. D., Glasius, M., Goldstein, A. H., Alves, E. G., Gomes, H., Gu, D., Guenther, A., Jathar, S. H., Kim, S., Liu, Y., Lou, S., Martin, S. T., McNeill, V. F., Medeiros, A., de Sá, S. S., Shilling, J. E., Springston, S. R., Souza, R. A. F., Thornton, J. A., Isaacman-VanWertz, G., Yee, L. D., Ynoue, R., Zaveri, R. A., Zelenyuk, A., and Zhao, C.: Urban pollution greatly enhances formation of natural aerosols over the Amazon
1025   rainforest, Nature Communications, 10, 1046, 10.1038/s41467-019-08909-4, 2019.

Shu, Y., and Atkinson, R.: Rate constants for the gas-phase reactions of O3 with a series of terpenes and OH radical formation from the O3 reactions with sesquiterpenes at 296±2 K, International Journal of Chemical Kinetics, 26, 1193-1205, 1994.

Shu, Y., and Atkinson, R.: Atmospheric lifetimes and fates of a series of sesquiterpenes, Journal of Geophysical
1030   Research: Atmospheres, 100, 7275-7281, https://doi.org/10.1029/95JD00368, 1995.

Stolzenburg, D., Fischer, L., Vogel, A. L., Heinritzi, M., Schervish, M., Simon, M., Wagner, A. C., Dada, L., Ahonen, L. R., Amorim, A., Baccarini, A., Bauer, P. S., Baumgartner, B., Bergen, A., Bianchi, F., Breitenlechner, M., Brilke, S., Buenrostro Mazon, S., Chen, D., Dias, A., Draper, D. C., Duplissy, J., El Haddad, I., Finkenzeller,

H., Frege, C., Fuchs, C., Garmash, O., Gordon, H., He, X., Helm, J., Hofbauer, V., Hoyle, C. R., Kim, C., Kirkby, J., Kontkanen, J., Kürten, A., Lampilahti, J., Lawler, M., Lehtipalo, K., Leiminger, M., Mai, H., Mathot, S., Mentler, B., Molteni, U., Nie, W., Nieminen, T., Nowak, J. B., Ojdanic, A., Onnela, A., Passananti, M., Petäjä, T., Quéléver, L. L. J., Rissanen, M. P., Sarnela, N., Schallhart, S., Tauber, C., Tomé, A., Wagner, R., Wang, M., Weitz, L., Wimmer, D., Xiao, M., Yan, C., Ye, P., Zha, Q., Baltensperger, U., Curtius, J., Dommen, J., Flagan, R. C., Kulmala, M., Smith, J. N., Worsnop, D. R., Hansel, A., Donahue, N. M., and Winkler, P. M.: Rapid growth of organic aerosol nanoparticles over a wide tropospheric temperature range, Proceedings of the National Academy of Sciences, 115, 9122-9127, 10.1073/pnas.1807604115, 2018.

Tarvainen, V., Hakola, H., Hellén, H., Bäck, J., Hari, P., and Kulmala, M.: Temperature and light dependence of the VOC emissions of Scots pine, Atmos. Chem. Phys., 5, 989-998, 10.5194/acp-5-989-2005, 2005.

van Eijck, A., Opatz, T., Taraborrelli, D., Sander, R., and Hoffmann, T.: New tracer compounds for secondary organic aerosol formation from β-caryophyllene oxidation, Atmospheric Environment, 80, 122-130, 2013.

Verma, S. K., Kawamura, K., Deshmukh, D. K., Haque, M. M., and Pavuluri, C. M.: Seasonal Characteristics of Biogenic Secondary Organic Aerosols Over Chichijima Island in the Western North Pacific: Impact of Biomass Burning Activity in East Asia, Journal of Geophysical Research: Atmospheres, 126, e2020JD032987, https://doi.org/10.1029/2020JD032987, 2021.

Von Hessberg, C., Von Hessberg, P., Pöschl, U., Bilde, M., Nielsen, O., and Moortgat, G.: Temperature and humidity dependence of secondary organic aerosol yield from the ozonolysis of β-pinene, Atmos. Chem. Phys, 9, 3583-3599, 2009.

Wagner, R., Bunz, H., Linke, C., Möhler, O., Naumann, K.-H., Saathoff, H., Schnaiter, M., and Schurath, U.: Chamber simulations of cloud chemistry: the AIDA Chamber, in: Environmental simulation chambers: application to atmospheric chemical processes, Springer, 67-82, 2006.

Wang, M., Yao, L., Zheng, J., Wang, X., Chen, J., Yang, X., Worsnop, D. R., Donahue, N. M., and Wang, L.: Reactions of atmospheric particulate stabilized Criegee intermediates lead to high-molecular-weight aerosol components, Environmental science & technology, 50, 5702-5710, 2016.

Weikl, F., Ghirardo, A., Schnitzler, J.-P., and Pritsch, K.: Sesquiterpene emissions from Alternaria alternata and Fusarium oxysporum: effects of age, nutrient availability, and co-cultivation, Scientific reports, 6, 22152, 2016.

Williams, L. R., Gonzalez, L. A., Peck, J., Trimborn, D., McInnis, J., Farrar, M. R., Moore, K. D., Jayne, J. T., Robinson, W. A., Lewis, D. K., Onasch, T. B., Canagaratna, M. R., Trimborn, A., Timko, M. T., Magoon, G., Deng, R., Tang, D., de la Rosa Blanco, E., Prévôt, A. S. H., Smith, K. A., and Worsnop, D. R.: Characterization of an aerodynamic lens for transmitting particles greater than 1 micrometer in diameter into the Aerodyne aerosol mass spectrometer, Atmos. Meas. Tech., 6, 3271-3280, 10.5194/amt-6-3271-2013, 2013.

Winterhalter, R., Herrmann, F., Kanawati, B., Nguyen, T. L., Peeters, J., Vereecken, L., and Moortgat, G. K.: The gas-phase ozonolysis of β-caryophyllene (C 15 H 24). Part I: an experimental study, Physical Chemistry Chemical Physics, 11, 4152-4172, 2009.

Witkowski, B., and Gierczak, T.: Early stage composition of SOA produced by α-pinene/ozone reaction: α-Acyloxyhydroperoxy aldehydes and acidic dimers, Atmospheric Environment, 95, 59-70, 2014.

1070

Wu, C., Bell, D. M., Graham, E. L., Haslett, S., Riipinen, I., Baltensperger, U., Bertrand, A., Giannoukos, S., Schoonbaert, J., El Haddad, I., Prevot, A. S. H., Huang, W., and Mohr, C.: Photolytically induced changes in composition and volatility of biogenic secondary organic aerosol from nitrate radical oxidation during night-to-day transition, Atmos. Chem. Phys., 21, 14907-14925, 10.5194/acp-21-14907-2021, 2021.

1075

Yasmeen, F., Vermeylen, R., Szmigielski, R., Iinuma, Y., Böge, O., Herrmann, H., Maenhaut, W., and Claeys, M.: Terpenylic acid and related compounds: precursors for dimers in secondary organic aerosol from the ozonolysis of α- and β-pinene, Atmos. Chem. Phys., 10, 9383-9392, 10.5194/acp-10-9383-2010, 2010.

Ye, Q., Wang, M., Hofbauer, V., Stolzenburg, D., Chen, D., Schervish, M., Vogel, A., Mauldin, R. L., Baalbaki, R., Brilke, S., Dada, L., Dias, A., Duplissy, J., El Haddad, I., Finkenzeller, H., Fischer, L., He, X., Kim, C., Kürten, A., Lamkaddam, H., Lee, C. P., Lehtipalo, K., Leiminger, M., Manninen, H. E., Marten, R., Mentler, B., Partoll, E., Petäjä, T., Rissanen, M., Schobesberger, S., Schuchmann, S., Simon, M., Tham, Y. J., Vazquez-Pufleau, M., Wagner, A. C., Wang, Y., Wu, Y., Xiao, M., Baltensperger, U., Curtius, J., Flagan, R., Kirkby, J., Kulmala, M., Volkamer, R., Winkler, P. M., Worsnop, D., and Donahue, N. M.: Molecular Composition and Volatility of Nucleated Particles from α-Pinene Oxidation between −50 °C and +25 °C, Environmental Science & Technology, 53, 12357-12365, 10.1021/acs.est.9b03265, 2019.

1080

1085

Zhao, Y., Zhang, R., Sun, X., He, M., Wang, H., Zhang, Q., and Ru, M.: Theoretical study on mechanism for O3-initiated atmospheric oxidation reaction of β-caryophyllene, Journal of Molecular Structure: THEOCHEM, 947, 68-75, 2010.

1090
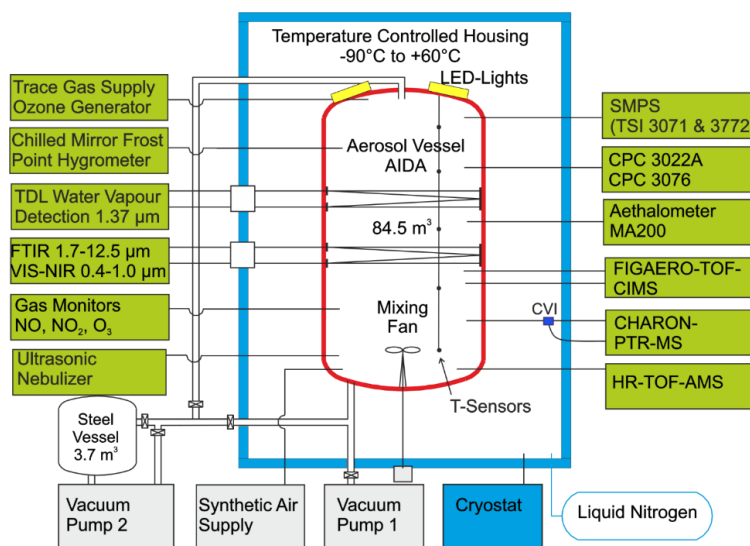
Fig. 1. Schematic of the AIDA simulation chamber and its instrumentation for this study.
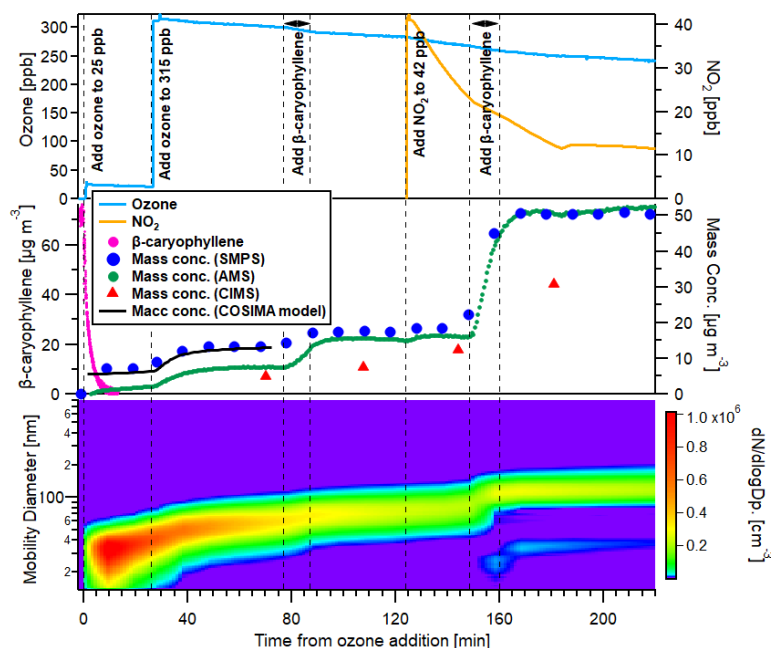
Fig. 2. Evolution of trace gases as well as particle mass & size for β-caryophyllene ozonolysis at 298K first without and then in presence of NO₂. The time axis is relative to the first addition of ozone. Top panel shows the concentration of ozone (blue) and NO₂ (yellow) as well as the experiment steps; middle panel shows the change of β-caryophyllene (pink), particle concentration from SMPS (blue dots) and COSIMA model (black line), AMS (green dots) and CIMS (red triangle); bottom panel shows the particle size distribution over the course of the whole experiment.
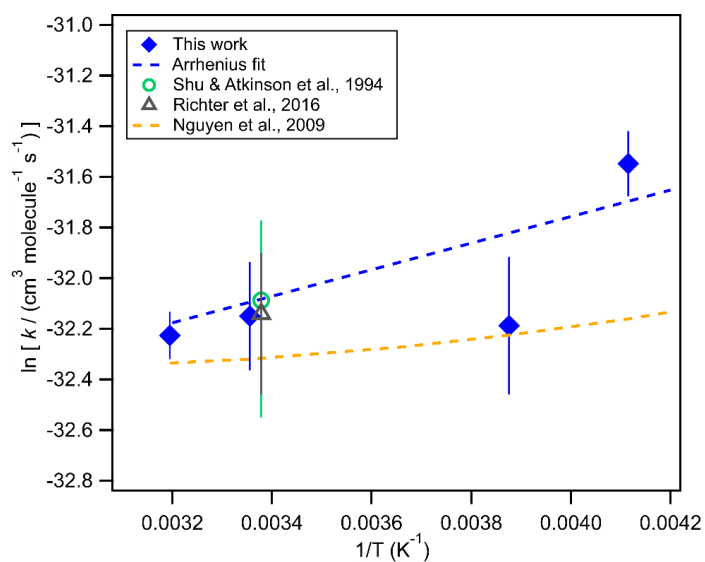
Fig. 3. Arrhenius plot of the rate coefficients determined for the reaction of ozone with the endocyclic double bond of β-caryophyllene (blue diamonds) compared to the values measured by Shu and Atkinson et al.,1994 (green circle) and Richter et al., 2016, at 296 K (grey triangle) as well as model calculations by Nguyen et al., 2009 (yellow dashed line). The blue dashed line is a fit to the rate coefficients determined in this work.

1105
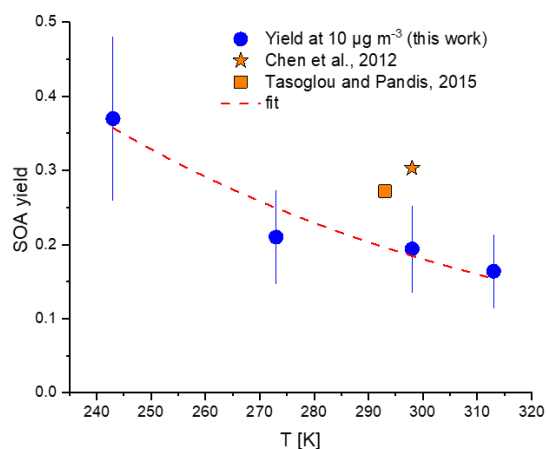
Fig. 4. SOA mass yield from β-caryophyllene ozonolysis at a constant total organic aerosol mass (M_{org}) of 10 μg m⁻³ for temperatures between 243 – 313 K from this study in comparison with literature data. The dashed line represents a single exponential fit to the data.Chen et al., 2012 used OH/CI scavenger and ammonium sulfate as seeds; Tasoglou and Pandis, 2015 used OH/Cl scavenger. Another comparison with literature data is given in Fig. S4.

1110
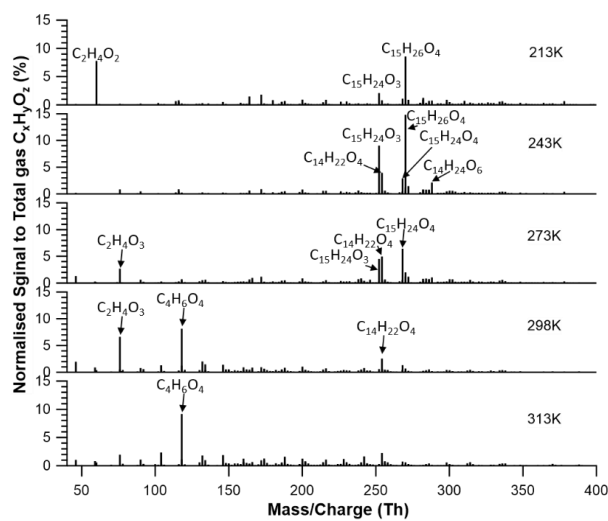
1115   **Fig. 5. Averaged CIMS gas phase mass spectra (background subtracted) for all temperatures, indicating the gas information when the SOA got stable in the absence of nitrogen oxids. The particle information sampled at the same time is given in Fig. 6 and Fig. 7.**
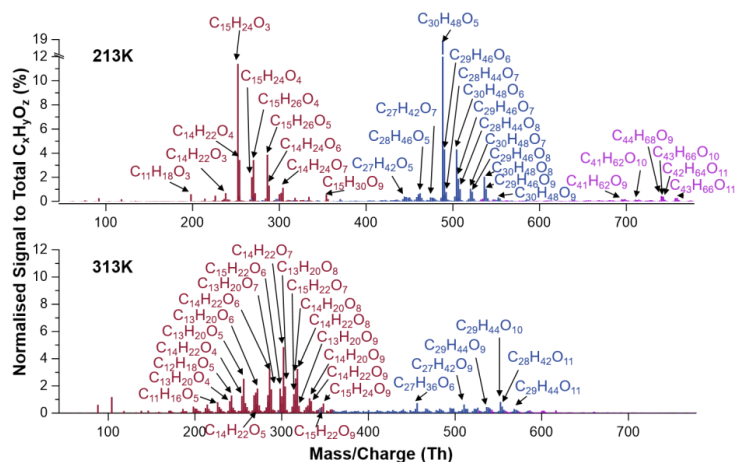
1120   **Fig. 6. CIMS mass spectra of particle phase compounds obtained from ozonolysis of β-caryophyllene without NO$_2$ at 213K (upper panel) and 313K (lower panel). Colours refer to monomeric (brown), dimeric (blue) and trimeric (purple) compounds, labels represent the assignment of individual molecules.**
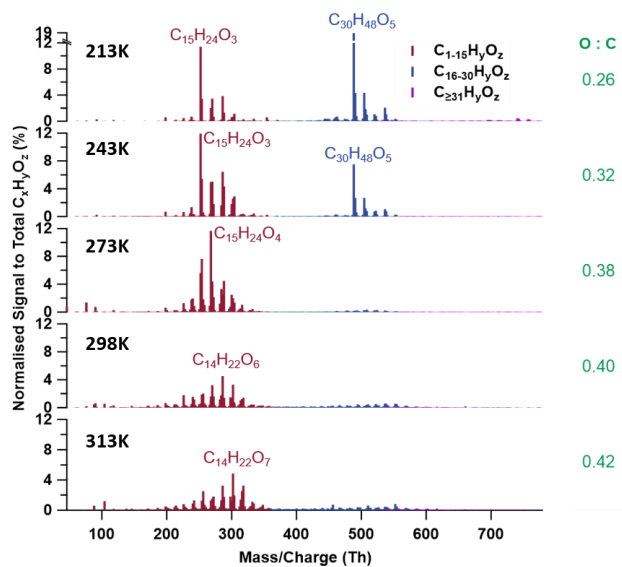
Fig. 7. CIMS mass spectra for particle phase compounds for all five temperatures (213 - 313K). Colours refer to monomeric (brown), dimeric (blue) and trimeric (purple) compounds. The table lists the signal-weighted bulk O:C ratios for each temperature. The mass to charge ratios in x-axis are subtracted by I⁻ ($m/z = 126.9$).
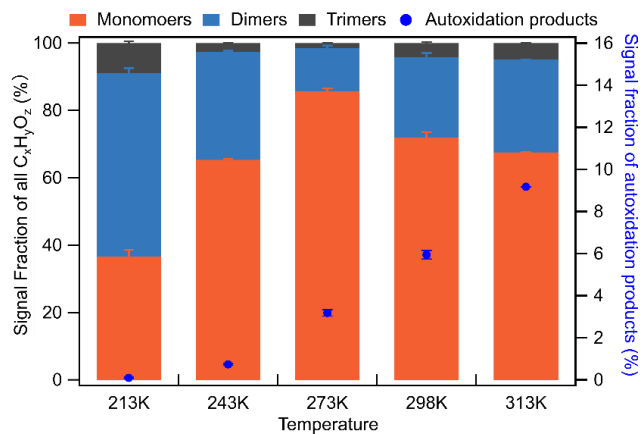
1130   **Fig. 8. Product groups contributing to SOA from ozonolysis of β-caryophyllene without NO₂ at temperatures between 213 – 313 K. Autoxidation-products calculation includes $C_{14}H_{22}O_{7,9}$, $C_{15}H_{22}O_{7,9}$ and $C_{15}H_{24}O_{7,9}$ identified in previous studies (Jokinen et al., 2016; Richters et al., 2016).**
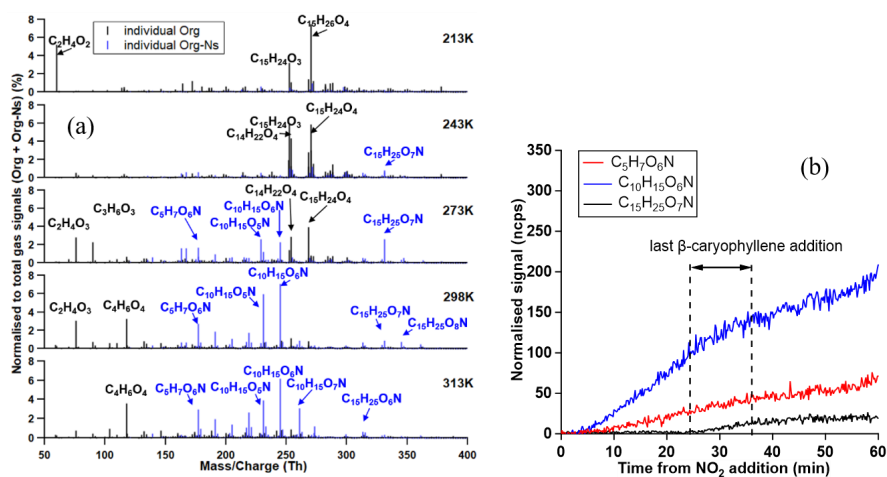
1135 **Fig. 9. CIMS gas phase mass spectra for all temperatures in the presence of NO₂ (a). These spectra correspond to the same time as the particle phase spectra shown in Fig. 12. Colours refer to compounds without nitrogen atoms (black) and compounds with one nitrogen atom (blue). The I- (*m/z* =126.9) was subtracted and here the mass/charge refers to the weight of the molecules. The panel (b) shows the FIGAERO-iodide-CIMS measurement for the signal change of three typical organonitrate molecules for C5 (C₅H₇O₆N, red line), C10 (C₁₀H₁₅O₆N, blue line) and C15 (C₁₅H₂₅O₇N,**
1140 **black line) corresponding to the evolution starting after NO₂ addition at 298K.**
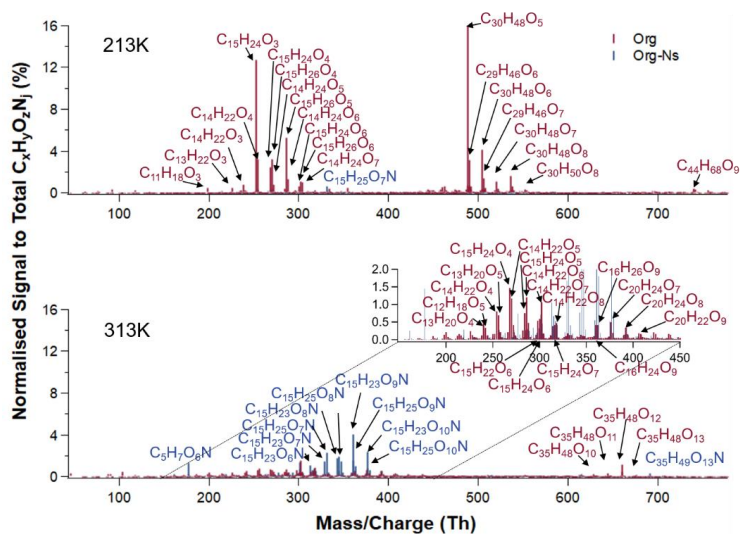
Fig. 10. CIMS mass spectra of particle phase compounds obtained from ozonolysis of β-caryophyllene in presence of nitrogen oxides at 213K (upper panel) and 313K (lower panel). Colours refer to compounds without nitrogen atoms (red) and compounds with one nitrogen atom (blue).

1145
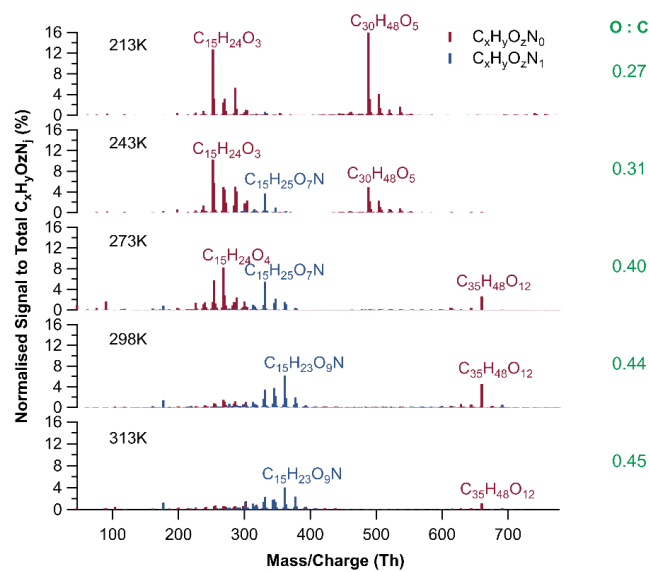
Fig. 11. CIMS mass spectra for particle phase compounds for all five temperatures (213 – 313 K). Colours refer to $C_xH_yO_zN_0$ (brown) and $C_xH_yO_zN_1$ (blue) compounds. The table lists the average O:C ratios for each temperature.

1150
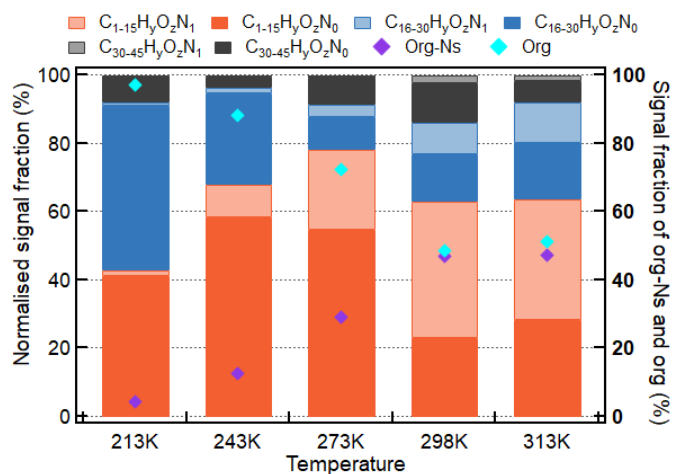
Fig. 12. Product groups (monomeric org, dimeric org, trimeric org, monomeric org-Ns, dimeric org-Ns, and trimeric org-Ns) contributing to SOA from ozonolysis of β-caryophyllene in presence of nitrogen oxides at temperatures between 213 – 313 K.

1155

Table1. Compilation of experimental conditions, O:C ratios, SOA densities, and yields

Exp. No.	T [K]	RH [%]	BCP [μg m^{-3}]	Total O$_3$ [ppb]	Total NO$_2$ [ppb]	NO$_3$ radicals [ppb]	SOA mass[+] (SMPS) [μg m^{-3}]	O:C (CIMS)	SOA density [g cm^{-3}]	SOA Yield [%]	BCA Yield [%]
1a	213	96	#	320	0	-	14.4±3.6	0.26	0.75±0.06	-	-
2a	243	88	15.8±3.1 (15.6±3.1[t])	317	0	-	4.5±1.1	0.32	0.86±0.14	28.5±8	11.1±7.3
3a	273	67	109.5±21.9	73	0	-	31.5±7.9	0.38	1.0±0.08	29.7±8	4.1±2.7
4a	298	27	65.0±13 (23.2±4.6[t])	325	0	-	13.6±3.4	0.41	1.09±0.12	20.9±6	0.8 ± 0.5 (4*)
5a	313	13	78.6±15.7	290	0	-	13.7±3.4	0.42	1.09±0.16[ass]	17.4±5	0.6±0.4
6a	243	59	65.0±13.0	6-505	0	-	-	-	-	-	-
7a	258	50	94±19	13-419	0	-	-	-	-	-	-
1b	213	96	#	320	27	-	13.9±3.5 (28.3±7.1[t])	0.27	-	-	-
2b	243	88	14.2± 2.8[t]	317	32	0.8	18.0±4.5 (52.5±13.1[t])	0.31	-	-	-
3b	273	67	109.5±21.9[t]	361	39	3.5	30.8±7.7 (62.4±15.6[t])	0.40	-	-	-
4b	298	27	27.9± 5.6[t]	325	42	5.3	32.1±8.0 (49.1±12.3[t])	0.44	-	-	-
5b	313	13	24.6±4.9[t]	290	46	5.6	21.8±5.5 (34.4±8.6[t])	0.45	-	-	-

*measured by (Jaoui et al., 2003); [+]SOA mass wall loss corrected; [t] following BCP addition calculated assuming a constant BCP addition rate in each experiment; #not detectable due to wall losses. [ass] assumed to have the same density as at 298K due to its large measurement uncertainty; BCA, β-caryophyllinic acid, regarded as a tracer of β-caryophyllene in the atmosphere.

1160